



# Size-dependent dynamics of the internal carbon pool drive isotopic vital effects in calcifying phytoplankton

Nishant Chauhan<sup>\*</sup>, Rosalind E.M. Rickaby

University of Oxford – Department of Earth Sciences, South Parks Road, Oxford OX1 3AN, UK

## ARTICLE INFO

Associate editor: Claire Rollion-Bard

### Keywords:

Vital effects  
Coccolithophores  
Carbon demand and supply  
Internal carbon pool  
Carbon residence time

## ABSTRACT

Isotopic offsets in biogenic calcite from equilibrium values can provide unique insights into the physiology and mechanisms of carbon regulation in calcifying phytoplankton. This study examines the impact of varying CO<sub>2</sub> (controlled via pH) on five coccolithophore species chosen for varied cell sizes, physiology, and calcification. The study investigates isotopic offsets in coccolith calcite and organic matter, in relation to carbon demand and supply ( $\mu/\text{CO}_2$ ). Species-specific CO<sub>2</sub> and/or pH optima for growth ( $\mu_{\text{opt}}$ ) were derived from variations in growth rates with varying CO<sub>2</sub> concentrations. Growth rates for all species declined with rising CO<sub>2</sub> (decreasing pH) due to H<sup>+</sup>-driven inhibition. *C. braarudii* and *C. leptoporus* exhibited  $\mu_{\text{opt}}$  at high CO<sub>2</sub> concentrations (suggesting high carbon-demand) and limited growth under low CO<sub>2</sub> (high pH) suggesting carbon limitation. Under low CO<sub>2</sub> supply, when growth rates were CO<sub>2</sub>-limited, both species exhibited coincident isotopic depletion in calcite and organic matter as a consequence of CO<sub>2</sub> diffusion into the cell that experienced no equilibration as a result of a highly depleted internal carbon pool. In these two species, isotopic values in calcite remained unaffected by growth rates and CO<sub>2</sub> concentration ( $\mu/\text{CO}_2$ ) when CO<sub>2</sub> was sufficient for optimal growth. *G. huxleyi* and *G. oceanica* displayed optima for growth ( $\mu_{\text{opt}}$ ) at low CO<sub>2</sub> concentrations and showed no growth limitation under low CO<sub>2</sub> (indicating low carbon-demand). Both species experienced depleted (negative) vital effects caused by an excess of CO<sub>2</sub> diffusion into the small internal carbon pool of the cell when diffusive carbon supply outpaced low demand (low  $\mu/\text{CO}_2$ ). Enriched (positive) vital effects were observed under low carbon supply and high demand, likely due to increased HCO<sub>3</sub><sup>-</sup> uptake and diffusive CO<sub>2</sub> loss from the intracellular carbon pool due to a lower intracellular pH than the seawater pH. *C. carterae* exhibited a  $\mu_{\text{opt}}$  at intermediate CO<sub>2</sub> concentrations and isotopically equilibrated intracellular carbon pool such that  $\delta^{13}\text{C}$  values in calcite and organic matter suggested a shared carbon pool. This study illustrates that pH and CO<sub>2</sub> driven vital effects and fractionation into organic matter indicate the residence time for carbon in the intracellular carbon pool, where the size of the pool is proportional to cell size. Due to the increased buffering afforded by a larger pool, *C. leptoporus* and *C. carterae* may have elevated intracellular pH which minimises CO<sub>2</sub> leakage, whereas vital effects in *G. huxleyi* and *G. oceanica* are caused by CO<sub>2</sub> diffusion in or out of their small internal carbon pool with limited buffering capacity owing to its small size.

## 1. Introduction

Stable isotopes in biogenic calcite offer insights into paleoclimate reconstructions spanning a sizeable portion of Earth's geological history and enhance our understanding of Biosphere-Geosphere interactions. However, “vital effects”, the isotopic offset from calcite precipitated in equilibrium, due to factors within the biomineralizing organism, often complicate the interpretation of climate signals in biologically mediated carbonate precipitation. These “vital effects” are caused by a multitude

of chemical, physical, and biological processes, which introduce deviations in the biogenic calcite from equilibrium and calculated inorganic compositions.

Purely inorganic calcite precipitation causes equilibrium fractionation effects, inducing isotopic fractionation between the solution and calcite due to differences in the strength of molecular bonding (Zeebe and Wolf-Gladrow, 2001). Additionally, thermodynamic factors stemming from environmental variables such as temperature can also contribute to the differences in molecular energies and impact

<sup>\*</sup> Corresponding author.

E-mail address: [nishant.chauhan@earth.ox.ac.uk](mailto:nishant.chauhan@earth.ox.ac.uk) (N. Chauhan).

<https://doi.org/10.1016/j.gca.2024.03.033>

Received 31 October 2023; Accepted 30 March 2024

Available online 1 April 2024

0016-7037/© 2024 The Author(s). Published by Elsevier Ltd. This is an open access article under the CC BY license (<http://creativecommons.org/licenses/by/4.0/>).

equilibrium fractionation. Urey (1947) first demonstrated the utility of temperature-related fractionation in foraminiferal calcite for paleo-temperature reconstruction.

McCrea (1950) established the relationship between solution pH and the isotopic composition of precipitating calcite. The study revealed the dependence of the calcite oxygen isotopic composition (referred to as  $\delta^{18}\text{O}$ ) on the concentration of  $\text{CO}_3^{2-}$  ions, which is proportional to pH. They showed that with increasing pH, as the abundance of  $\text{CO}_3^{2-}$  ion increases, the  $\delta^{18}\text{O}$  of the precipitating calcite becomes more depleted. This is because the  $\delta^{18}\text{O}$  of  $\text{CO}_3^{2-}$  is isotopically depleted compared to the other carbonate species and the proportion of  $\text{CO}_3^{2-}$  ion within the DIC increases with rising pH (Zeebe, 1999).

The  $\delta^{18}\text{O}$  – pH relationship has since gained significance as the isotopic composition of temperature-corrected calcite could function as a proxy for seawater pH or carbonate ion (Spero et al., 1997). Conversely, pH-mediated effects on the isotopic composition of calcite could interfere with the temperature signal. Subsequent advancements unveiled the mechanism of isotopic equilibration in the  $\text{H}_2\text{O}$ -DIC- $\text{CaCO}_3$  system for the carbon and oxygen isotopes which have been explained here briefly (referred to as  $\delta^{13}\text{C}$  and  $\delta^{18}\text{O}$  respectively; Zeebe and Wolf-Gladrow, 2001).

Isotopic equilibration in  $\delta^{13}\text{C}$  is controlled by interconversion reactions between  $\text{CO}_2$ ,  $\text{HCO}_3^-$ , and  $\text{CO}_3^{2-}$  driven by the different binding strengths of the carbon in each molecule. Among these reactions is the hydration/hydroxylation of  $\text{CO}_2$  to  $\text{HCO}_3^-$  and its reverse, which is the rate limiting step in carbon isotopic equilibration. The hydration reaction can cause the  $\text{HCO}_3^-$  to be (-)13 ‰ more depleted in  $\delta^{13}\text{C}$  than  $\text{CO}_2$ , whereas the dehydration reaction can cause the  $\text{CO}_2$  to be about (-)22 ‰ more depleted in  $\delta^{13}\text{C}$  than  $\text{HCO}_3^-$  (O'Leary et al., 1992; Zeebe and Wolf-Gladrow, 2001). The slow carbon isotopic equilibration rate between  $\text{CO}_2$  and  $\text{HCO}_3^-$  can cause a significant depletion in the isotopic composition of the precipitating calcite. A depletion of (-)10 – 15 ‰ in the  $\delta^{13}\text{C}$  and (-)4 ‰ in  $\delta^{18}\text{O}$  of corals was reported to be caused by such a mechanism (McConnaughey, 1989a).

Carbonic anhydrase (CA) is suggested to significantly influence the rate of hydration/hydroxylation between  $\text{CO}_2$  and  $\text{HCO}_3^-$  (the rate limiting step) by catalysing this reaction, therefore, allowing faster equilibration in both  $\delta^{13}\text{C}$  and  $\delta^{18}\text{O}$  and alleviating kinetic fractionation effects caused by hydration/hydroxylation of  $\text{CO}_2$  to  $\text{HCO}_3^-$  (Chen et al., 2018; Thaler et al., 2017; Uchikawa and Zeebe, 2012).

Isotopic equilibration in  $\delta^{18}\text{O}$  occurs through the equilibration between  $\text{CO}_2$  –  $\text{HCO}_3^-$  –  $\text{CO}_3^{2-}$  (DIC) through interconversion reactions described above and equilibration between  $\text{H}_2\text{O}$  and  $\text{CO}_2$ , which occurs more slowly than that for carbon isotopes.  $\delta^{18}\text{O}$  isotopic equilibration needs to take place between one oxygen atom in  $\text{H}_2\text{O}$  and three atoms in each carbonate and bicarbonate molecule ( $\text{HO-COO}^-$  and  $\text{COO}^{2-}$ ), and two atoms in the  $\text{CO}_2$  molecule. Isotopic equilibration between  $\text{H}_2\text{O}$  and DIC is also influenced by pH, as the proportion of DIC present as  $\text{CO}_2$  becomes significantly low at high pH. For instance, the time required for 99 % isotopic equilibration in the carbonate system of seawater can take about 12.4 h at pH 8 at 19 °C (Zeebe and Wolf-Gladrow, 2001). Under alkaline conditions (common during calcite precipitation), isotopic equilibration is even slower, and can cause significant deviations in the calcite isotopes from equilibrium values, causing kinetic isotopic effects (Adkins et al., 2003; McConnaughey, 1989a, 1989b, 2003).

Kinetic isotope effects in  $\delta^{13}\text{C}$  and  $\delta^{18}\text{O}$  caused by disequilibrium in the DIC- $\text{H}_2\text{O}$  system have also spurred investigations into kinetic fractionation in inorganic  $\text{CaCO}_3$  due to calcite crystal growth rate, where a high calcite-crystal growth rate causes isotopic depletion in the  $\delta^{13}\text{C}$  and  $\delta^{18}\text{O}$  of calcite due to non-equilibrium fractionation factors (Watkins et al., 2013). Additionally,  $\text{CO}_2$  diffusion to the site of precipitation in an organism can lead to mass-dependent kinetic isotope effects (Eiler, 2007; Schauble, 2004). According to the kinetic diffusion model, lighter isotopes (e.g.,  $^{12}\text{C}^{16}\text{O}^{16}\text{O}$ ) diffuse more rapidly than their heavier counterparts (e.g.,  $^{13}\text{C}^{16}\text{O}^{16}\text{O}$  and  $^{12}\text{C}^{18}\text{O}^{16}\text{O}$ ; Wanner & Hunkeler, 2019). Although a limited number of studies have attempted to quantify

the extent of isotopic depletion caused by aqueous-phase  $\text{CO}_2$  diffusion, experimental evidence suggests a potential depletion of (-)0.7 to (-)0.87 ‰ in  $\delta^{13}\text{C}$  (Jähne et al., 1987; O'Leary, 1984) and (-)1.6 ‰ in  $\delta^{18}\text{O}$  (Thiagarajan et al., 2011).

Furthermore, biogenic calcite can also be influenced by metabolic processes such as respiration and photosynthesis. Isotopic changes due to the preferential uptake of depleted  $\text{CO}_2$  by RuBisCO, the key enzyme in photosynthesis have been highlighted in  $\delta^{13}\text{C}$  (McClelland et al., 2017; McConnaughey, 1989a). However, it is worth noting that fractionation by RuBisCO is recognised in both  $\delta^{13}\text{C}$  and  $\delta^{18}\text{O}$  (Guy et al., 1993; Tcherkez et al., 2006).

Understanding the variability of vital effects with environmental factors can provide significant additional information about the physiology of biomineralizing organisms. Noteworthy candidate organisms are coccolithophores, offering a promising avenue for paleoenvironmental reconstruction owing to their geological history spanning over 200 Ma (Bown et al., 2004). Much like foraminifera, stable isotopes in different species of coccolith calcite are known to display distinct offsets from equilibrium which have been used for the reconstruction of past environments (Bolton and Stoll, 2013; Claxton et al., 2022; Dudley et al., 1986; Hermoso et al., 2020).

Prior studies have suggested that vital effects in coccolithophores diminish as carbon supply increases, but species-specific deviations from abiogenic calcite occur at low DIC/ $\text{CO}_2$  concentrations (Hermoso et al., 2016a; McClelland et al., 2017; Rickaby et al., 2010). These studies simulated an increase in  $\text{CO}_2$  by increasing DIC concentrations at a constant pH. Moreover, they suggested a mechanistic link between the magnitude of coccolith vital effects and the species-specific ratio of particulate inorganic carbon (PIC) to particulate organic carbon (POC) and carbon demand vs supply (analogous to  $\mu/\text{CO}_2$ ).

It remains unclear whether the physiological and isotopic effects observed stem from an increase in  $\text{CO}_2$ , from changes in DIC concentration, or from an interplay of both factors. This is because vital effects in coccolithophore calcite were reported to become increasingly depleted with increasing  $\text{CO}_2$  (Hermoso, 2015), where  $\text{CO}_2$  was modified through pH manipulation at constant DIC concentration. This discrepancy indicates that the isotopic response of coccolithophores may vary depending on the specific parameters of the manipulated carbonate chemistry and on the effect of those chemical manipulations on their physiology.

In the diffusive model for organic isotopic fractionation, isotopic fractionation in organic matter increases with  $\text{CO}_2$  concentration but can be affected by growth rate (Laws et al., 1995; Rau et al., 1996). Accordingly, carbon demand to supply (denoted by  $\mu/\text{CO}_2$ ) has been correlated with isotopic fractionation in the organic matter and attributed to Rayleigh fractionation of an internal pool of carbon and used as a proxy for past  $p\text{CO}_2$  (Henderiks and Pagani, 2008; Pagani, 2002). This correlation comes with limitations due to factors that impact the relationship between isotopic fractionation and  $\mu/\text{CO}_2$ , such as active carbon uptake (Keller and Morel, 1999; Stoll et al., 2019; Tchernov et al., 2014).

There have been few studies reporting isotopic fractionation in both calcite and organic matter, and in  $\delta^{13}\text{C}$  and  $\delta^{18}\text{O}$  simultaneously. The carbon demand to supply models in coccolith calcite (McClelland et al., 2017) and organic matter (Rau et al., 1996) suggest that this parameter, possibly with active bicarbonate uptake, plays a crucial role in understanding vital effects and their relationship with species-specific coccolithophore physiology. Further investigation is needed to understand the relationship between isotopic fractionation in the calcite and organic matter of coccolithophores and seawater carbonate chemistry.

This study delves into the effects of pH and  $\text{CO}_2$  variations on isotopic signatures within coccoliths and organic matter. Through dilute batch cultures, stable isotopes in calcite and organic matter of five coccolithophore species of varying cell sizes, carbon demands, and PIC:POC ratios were investigated to understand the mechanisms of carbon regulation and isotopic fractionation in calcifying phytoplankton. The

results obtained from this study will provide a context within which size-separated coccolith fractions can be interpreted during paleoclimate reconstructions that use coccolithophore calcite and organic matter isotopes specifically pointing to periods when carbon limitation of different size fractions emerged (e.g., González-Lanchas et al., 2021; Bolton et al., 2016). Moreover, the broader application of the findings of this study will be useful in constructing numerical cell models to quantify the fluxes of carbon and calcium, and intracellular reservoirs, involved in coccolithophore calcification (Holtz et al., 2017, 2015).

## 2. Methodology

### 2.1. Coccolithophore Culturing

Live coccolithophore monocultures were sourced from the Roscoff Culture Collection (<https://www.roscoff-culturecollection.org>) and the Marine Biological Association (MBA, <https://www.mba.ac.uk>). Strains RCC 1198 (*Coccolithus braarudii*), RCC 1130 (*Calcidiscus leptoporus*), RCC 1314 (*Gephyrocapsa oceanica*), PLY 837 (*Gephyrocapsa huxleyi*, morphotype A; Bendif et al., 2019), and PLY 406 (*Chrysothila carterae*) were grown in filter-sterilised artificial seawater prepared using the Synthetic Ocean Water (SOW) recipe from Aquil\* synthetic medium (Price et al., 1989), modified from Morel et al. (1979) with a starting constant DIC concentration of  $\sim 2100 \mu\text{mol KgSW}^{-1}$ . These species were selected based on their unique physiological characteristics. For instance, *C. carterae* is a coastal species with a large cell size and small PIC:POC ratio (Houdan et al., 2004). PIC:POC ratios were taken from previously published data (Table S1, Supplementary Information; Gafar et al., 2019a; McClelland et al., 2017). *G. huxleyi* and *G. oceanica* are ubiquitous bloom forming species that are widely studied in the paleoclimatic records and the modern ocean (González-Lanchas et al., 2021; Paasche, 1964; Wheeler et al., 2023). These species have small cell sizes and intermediate PIC:POC ratios. *C. leptoporus* and *C. braarudii* have long ancestral lineages and are key calcifiers in the modern ocean (Agnini et al., 2014; Backman, 1980; Ridgwell, 2005; Young, 1998). These species have large cell sizes, and relatively higher PIC:POC ratios (Table S1). The SOW was enriched with  $100 \mu\text{mol kg}^{-1}$  nitrate,  $6.25 \mu\text{mol kg}^{-1}$  phosphate, and  $27 \mu\text{mol kg}^{-1}$  silicate, supplemented with vitamins based on the *f/2* protocol (Guillard and Ryther, 1962) and trace metals according to the *K/2* protocol (Keller et al., 1987; Keller and Guillard, 1985), with modifications according to (Rickaby et al., 2010, Supplementary Material). pH was adjusted using 1N NaCl and 1N HCl and measured with a 3-point calibrated benchtop pH meter (Mettler Toledo SevenEasy). The seawater was filtered through a sterile 0.22  $\mu\text{m}$  Merck Steritop® bottle top filter, UV sterilised, and filled into acid-clean, sterile 2.3L polycarbonate bottles with no headspace.

Dilute batch cultures were employed, with a maximum 5 % change in [DIC] as recommended by (Langer et al., 2006; LaRoche et al., 2010; Rickaby et al., 2010; Hermoso, 2015; Supplementary Material). Cultures were grown in triplicate within a PHCbi MLR-352 Climate Chamber at  $17 \pm 0.1 \text{ }^\circ\text{C}$ . A 14-hour light:10-hour dark cycle was maintained, with the photon flux density ranging between 55 and  $80 \mu\text{mol m}^{-2} \text{ s}^{-1}$  during the light phase, depending on the position relative to the light source, which was randomised during the acclimatisation and experiment incubation phase. The strains were acclimated in the experimental media for a minimum of 14 generations (2 subsequent batch cultures of  $\sim 7$  generations each, transferred at mid-exponential growth) prior to their use as initial inoculates for the main experiment. Culture bottles were gently shaken daily and opened for less than a minute each to measure growth. Only 600  $\mu\text{L}$  of culture was extracted at once yielding a negligible effect on gas exchange and headspace.

Cell counts were measured using a Beckman Coulter Counter Z2 analyser. Isotopic measurements were conducted on the day of optimal cell density. All measurements were taken at the same time of day, starting 6 h after the beginning of the light phase, and lasting approximately 2 h. Coccusphere sizes were measured using SEM images

obtained on a Zeiss Sigma 300 FEG-SEM.

### 2.2. Measurement of growth

Specific growth rates were calculated based on in vivo log change in chlorophyll fluorescence per day using a TECAN Spark® Multimode Microplate Reader (excitation =  $485 \pm 20 \text{ nm}$ , emission =  $680 \pm 30 \text{ nm}$ ; Andersen, 2005). The specific growth rate ( $\mu$ ) was determined using the following equation:

$$\mu = \frac{\ln Chl flo_f - \ln Chl flo_i}{\Delta t}$$

Here, *Chl flo<sub>f</sub>* represents the blank-corrected chlorophyll fluorescence of the cell culture on the harvest day, *Chl flo<sub>i</sub>* represents the blank-corrected chlorophyll fluorescence one or two days before cell harvest, and  $\Delta t$  is the difference in days between the two measurements. Sterile culturing media was used as blanks. See Methods (Supplementary Material) for an overview of the challenges faced in this study with traditional cell counting methods at such dilute concentrations to justify in vivo log change in chlorophyll fluorescence per unit time being used for measuring specific growth rates.

### 2.3. Calculation of carbonate chemistry parameters

To determine pH, alkalinity, and DIC drift, approximately 12 mL of seawater sample was collected on the day of inoculation and at harvest after filtering through a 0.22  $\mu\text{m}$  syringe filter unit and stored in Labco Exetainer® vials with no headspace. The seawater samples were titrated in technical duplicates with a 0.01N HCl standardized solution on a Metrohm 916 Ti-Touch titrator to determine Total Alkalinity (TA) and pH. The pH probe was calibrated daily using NIST standard reference material (Thermo Scientific), and the precision and accuracy of the machine were assessed using Dickson CO<sub>2</sub> in seawater reference material (Batch 126, 197) provided by A. Dickson, Scripps Institution of Oceanography, La Jolla, CA. See Methods (Supplementary Material) for an overview of the precision and accuracy of the Dickson standards. Carbonate chemistry parameters were calculated using CO2Sys v2.1 (Pierrot et al., 2006) with the measured pH, TA, temperature, and calculated initial phosphate and silicate concentrations. The  $K_1$  and  $K_2$  constants were obtained from Mehrbach et al. (1973) and refit by Dickson & Millero (1987).

### 2.4. Isotopic measurements

For the analysis of  $\delta^{13}\text{C}$  of organic matter ( $\delta^{13}\text{C}_{\text{ORG}}$ ), 200 mL (per technical replicate) of culture was filtered through pre-combusted (450  $^\circ\text{C}$ , overnight) GF/F filters, washed with sterile seawater, acidified using 230  $\mu\text{L}$  of 0.1N HCl and oven-dried overnight at 40  $^\circ\text{C}$ . Samples were analysed on an Elementar Vario Isotope Select Elemental Analyser linked to an Isoprime 100 continuous flow IRMS at the Stable Isotope Ratio Mass Spectrometry Laboratory, School of Ocean and Earth Science, University of Southampton, National Oceanography Centre in Southampton, UK.

To measure  $\delta^{13}\text{C}$  and  $\delta^{18}\text{O}$  of coccolith calcite ( $\delta^{13}\text{C}_{\text{Coccolith}}$ ,  $\delta^{18}\text{O}_{\text{Coccolith}}$ ), approximately 600 mL of culture was filtered on a polycarbonate filter with a 0.8  $\mu\text{m}$  pore size. The collected material was cleaned according to (Lee et al., 2016, Supplementary Material). Internal standards were treated in the same manner as samples to evaluate the isotopic offset from absolute values due to cleaning.

For  $\delta^{13}\text{C}$  and  $\delta^{18}\text{O}$  of DIC ( $\delta^{13}\text{C}_{\text{DIC}}$  and  $\delta^{18}\text{O}_{\text{DIC}}$ ), culturing media was collected on the harvest day in the same way as the alkalinity samples. All calcite and DIC samples were analysed on a Thermo Delta V Advantage at the Stable Isotope Laboratory, Department of Earth Sciences, University of Oxford.

$\delta^{13}\text{C}$  of CO<sub>2</sub> was calculated from  $\delta^{13}\text{C}_{\text{DIC}}$  and the absolute temperature ( $T_K$ ) according to Mook et al. (1974) and the following equation

taken from Rau et al. (1996)

$$\delta^{13}C_{CO_2} = \delta^{13}C_{DIC} + 23.644 - (9701.5/T_k)$$

$\delta^{13}C$  of inorganic calcite ( $\delta^{13}C_{INORG}$ ) was calculated as  $\delta^{13}C_{DIC} + 1$  (Romanek et al., 1992) and  $\delta^{18}O_{INORG}$  was calculated to be  $-0.72$  ‰ V-PDB, based on the equation from Kim & O'Neil (1997) and Watkins et al. (2013) for a temperature of  $17$  °C and the  $\delta^{18}O$  of the seawater of  $0$  ‰ V-SMOW (Table S2, Supplementary Material). The effect of pH was considered from Zeebe (1999), where the  $\delta^{18}O$  of the precipitating calcite becomes lighter (depleted) with increasing pH as a consequence of the increasing proportion of the isotopically depleted  $CO_3^{2-}$ .

Reproducibility of replicated standards (NBS 18 and NBS 19) was always better than  $0.07$  ‰ VPDB for  $\delta^{13}C_{Calcite}$  and better than  $0.11$  ‰ VPDB for  $\delta^{18}O_{Calcite}$ . In addressing the impact of the cleaning process on isotopic values, an internal calcite standard was employed to account for offsets. The cleaning process resulted in a depletion of  $(-0.13$  ‰ in  $\delta^{13}C_{Calcite}$  values relative to the expected absolute values, while  $\delta^{18}O_{Calcite}$  values exhibited a corresponding enrichment of  $(+0.04$  ‰. The standard error associated with isotopic analysis using external standards found from the influence of the cleaning process on the absolute isotopic values of the internal standard was non-significant. The influence of sample treatment with similar magnitudes has been documented in prior studies (McConnaughey, 1989a). A comprehensive examination using Scanning Electron Microscopy did not reveal any

indications of inorganic  $CaCO_3$  overgrowth or coccolith dissolution after cleaning. For  $\delta^{13}C$  values of cellular organic matter ( $\delta^{13}C_{ORG}$ ), reproducibility on replicated standards (USGS 40 and 41a) was  $0.00 - 0.04$  ‰ VPDB for USGS 40 and  $0.05 - 0.43$  ‰ VPDB for USGS 41a.

### 3. Results

#### 3.1. Carbonate chemistry

During the dilute batch culture experiments, the average change in dissolved inorganic carbon concentration, [DIC], was approximately  $4.7$  ‰, with an average pH drift of  $0.04$  units. We used the initial alkalinity and pH values to compute and visualise other carbonate chemistry parameters, such as  $CO_2$  concentration (hereafter  $[CO_2]$ ). It is noted that the method of altering carbonate chemistry (through acid/base addition,  $CO_2$  bubbling, or changing DIC concentration) can impact species-specific responses to varying carbonate conditions (Bach et al., 2013; Hoppe et al., 2011; Iglesias-Rodriguez et al., 2008; Kottmeier et al., 2016a,b). The observed responses in this study are a consequence of modifications in both  $[CO_2]$  and  $[H^+]$ .

#### 3.2. Effect of $[CO_2]$ and pH on growth rates

All species consistently exhibited a decrease in growth rate

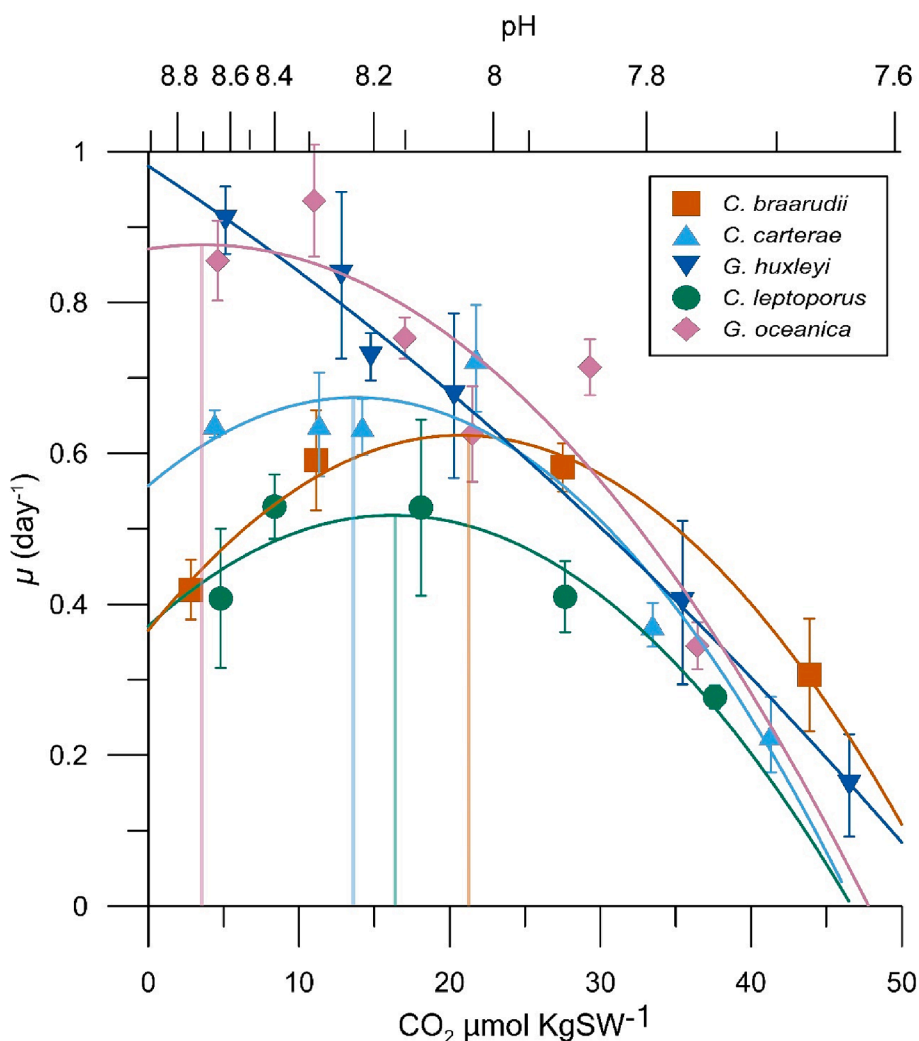


Fig. 1. Growth rates ( $day^{-1}$ ) for *C. braarudii* (■), *C. leptoporus* (●), *C. carterae* (▲), *G. huxleyi* (▼), and *G. oceanica* (◆). Each point is an average of 3 biological replicates. The curved lines represent 2nd-degree polynomial fits. Vertical bars indicate maximum growth rates ( $\mu_{opt}$ ), defined as the maximum of the polynomial fit curve. A plot of growth rates of all biological replicates can be found in the Supplementary Material (Fig. S3).

(minimum of  $\sim 0.2 \text{ day}^{-1}$ ) when exposed to high  $[\text{CO}_2]$  and low pH ( $\text{CO}_2 \geq 40 \mu\text{mol kg}^{-1}$ ,  $\text{pH} < 7.75$ ), while species-specific effects were observed at low  $[\text{CO}_2]$  (high pH; Fig. 1). These observed changes in growth rates are in line with previous research findings, as all species exhibited an optimum growth curve in response to variable  $[\text{CO}_2]$  and/or pH (Gafar et al., 2019b; Kottmeier et al., 2022).

The estimates for growth rate optimum ( $\mu_{\text{opt}}$ ) for  $\text{CO}_2$  and/or pH differed among species: *C. leptoporus* exhibited a modelled  $\mu_{\text{opt}}$  at  $16.3 \mu\text{mol kg}^{-1}$  (pH 8.1), *C. braarudii* at  $21.05 \mu\text{mol kg}^{-1}$  (pH 8.02), *C. carterae* at  $13.5 \mu\text{mol kg}^{-1}$  (pH 8.22), and *G. oceanica* at  $3.5 \mu\text{mol kg}^{-1}$  (pH 8.7). *G. huxleyi* did not reach a  $\text{CO}_2$  optimum for growth ( $< 5 \mu\text{mol kg}^{-1}$ ,  $\text{pH} > 8.8$ ).

*G. huxleyi* exhibited the highest growth rate of  $0.91 \text{ d}^{-1}$  at  $[\text{CO}_2]$  of  $5.1 \mu\text{mol kg}^{-1}$  (pH 8.6) and continually declined with increasing  $[\text{CO}_2]$  (Fig. 1). Similarly, maximum  $\mu$  for *G. oceanica* was  $0.94 \text{ d}^{-1}$  at  $[\text{CO}_2]$   $11 \mu\text{mol kg}^{-1}$  (pH 8.3) and growth rates declined with increasing  $\text{CO}_2$  (decreasing pH). Growth rates for *C. carterae* plateaued for  $[\text{CO}_2]$  below  $22 \mu\text{mol kg}^{-1}$  (pH 8.05). *C. braarudii* showed maximum  $\mu$  between  $[\text{CO}_2]$   $10\text{--}30 \mu\text{mol kg}^{-1}$  (pH 7.9–8.3) of  $\sim 0.58 \text{ d}^{-1}$  and showed declining  $\mu$  at higher and lower  $[\text{CO}_2]$ . Overall, *C. leptoporus* showed the lowest  $\mu$  in

comparison to other species at all  $[\text{CO}_2]$  conditions and we observed significant cell clumping at  $[\text{CO}_2] \sim 40 \mu\text{mol kg}^{-1}$  (pH 7.7). Similar observations have previously been reported for *C. leptoporus* (Langer and Bode, 2011).

Declining growth rates with increasing  $[\text{CO}_2]$  (decreasing pH) align with some studies (e.g., Gafar et al., 2019; Kottmeier et al., 2022; Krug et al., 2011), but differ from others (e.g., Langer et al., 2009; Rickaby et al., 2010; Hermoso et al. 2016) where growth rates did not change significantly with increasing  $[\text{CO}_2]$ . This may be owing to carbonate chemistry parameters in these studies being manipulated through either  $\text{CO}_2$  bubbling or DIC addition, instead of pH manipulation as in this study. Culture conditions, such as temperature, light intensity, nutrient concentration, seawater composition and irradiance cycles can also affect coccolithophore sensitivity to changing carbonate chemistry (Bach et al., 2015; Rokitta and Rost, 2012; Sett et al., 2014; Zhang and Gao, 2021; Zondervan et al., 2002). Growth rates can be compared between experiments within this study to understand species-specific and interspecific responses. Significant changes in coccosphere size were only observed in *C. carterae*, where coccosphere diameter increased from  $\sim 12 \mu\text{m}$  to  $\sim 19 \mu\text{m}$  with increasing  $[\text{CO}_2]$  (Fig. S6, Supplementary

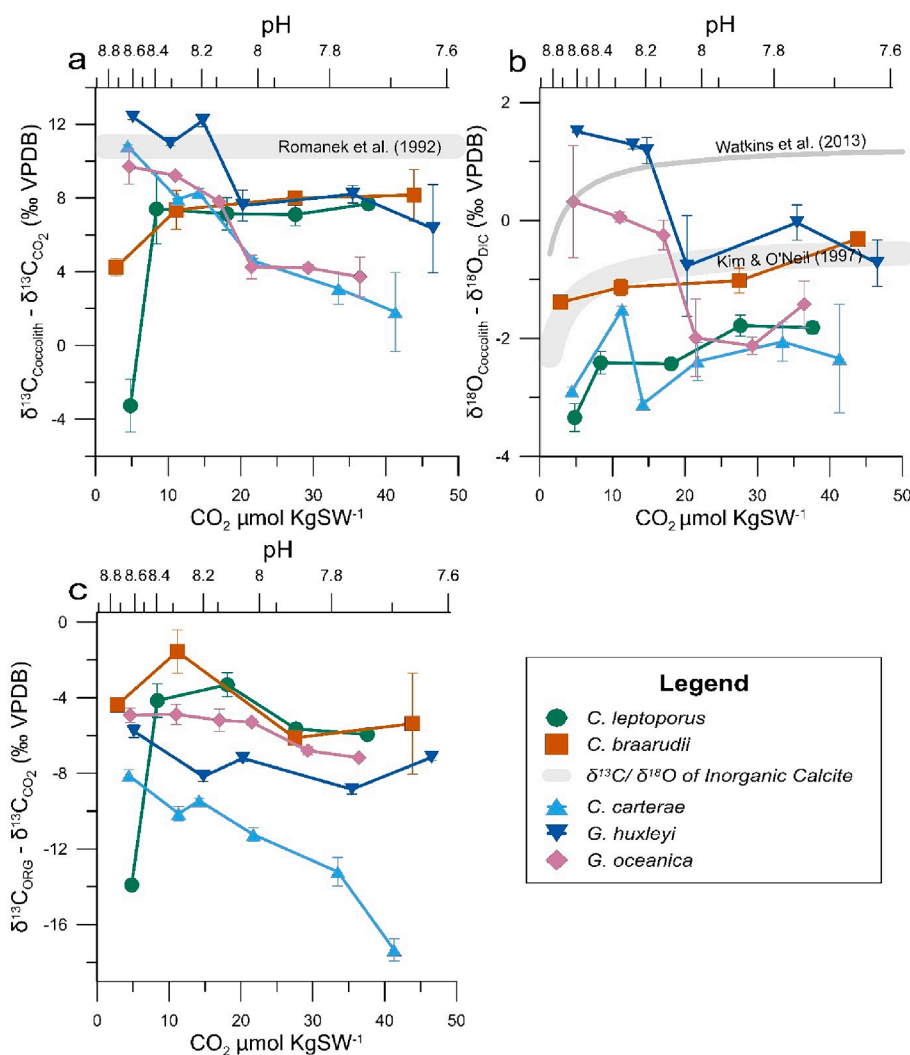


**Fig. 2.** (a)  $\Delta^{13}\text{C}_{\text{Coccolith}}$  ( $\delta^{13}\text{C}_{\text{Coccolith}} - \delta^{13}\text{C}_{\text{CO}_2}$ ), (b)  $\Delta^{18}\text{O}_{\text{Coccolith}}$  ( $\delta^{18}\text{O}_{\text{Coccolith}} - \delta^{18}\text{O}_{\text{DIC}}$ ), (c)  $\Delta^{13}\text{C}_{\text{ORG}}$  values ( $\delta^{13}\text{C}_{\text{ORG}} - \delta^{13}\text{C}_{\text{CO}_2}$ ) for *C. braarudii* (■), *C. leptoporus* (●), *C. carterae* (▲), *G. huxleyi* (▼), and *G. oceanica* (◆). Note the change in y-axes. Each data point signifies an average of 3 biological replicates, each with 3 replicate measurements. Measurements for each biological replicate can be found in the Supplementary Material (Fig. S4). Error bars represent one standard deviation. The grey line in (a) and (b) represents isotope values for inorganic calcite derived from (Kim and O’Neil, 1997; Romanek et al., 1992; Watkins et al., 2013).  $\delta^{18}\text{O}_{\text{Inorganic Calcite}}$  values are adjusted for pH according to (Zeebe, 1999).  $\delta^{18}\text{O}$  values for Inorganic Calcite from Watkins et al. (2013) represent closest  $\delta^{18}\text{O}$  values to thermodynamic equilibrium, while  $\delta^{18}\text{O}$  values for Inorganic Calcite from Kim and O’Neil (1997) represent inorganic  $\delta^{18}\text{O}$  values influenced by kinetic isotope effects. Note that although the relationship between  $\delta^{18}\text{O}$  and pH is linear, between  $\delta^{18}\text{O}$  and  $\text{CO}_2$ , it is logarithmic.

Material).

### 3.3. Stable isotopes

The carbon and oxygen isotopic composition of the coccolith calcite, denoted as  $\Delta^{13}\text{C}_{\text{Coccolith}}$  and  $\Delta^{18}\text{O}_{\text{Coccolith}}$  were plotted in the form of  $\delta^{13}\text{C}_{\text{Coccolith}} - \delta^{13}\text{C}_{\text{CO}_2}$  and  $\delta^{18}\text{O}_{\text{Coccolith}} - \delta^{18}\text{O}_{\text{DIC}}$  values, respectively (Fig. 2a,b). Carbon isotopes of the organic matter are represented as  $\Delta^{13}\text{C}_{\text{ORG}} = \delta^{13}\text{C}_{\text{ORG}} - \delta^{13}\text{C}_{\text{CO}_2}$ , ‰ VPDB. This allowed the quantification of the true isotopic fractionation relative to DIC, e.g.,  $\Delta^{13}\text{C}_{\text{Coccolith}} = \delta^{13}\text{C}_{\text{Coccolith}} - \delta^{13}\text{C}_{\text{CO}_2}$ , ‰ VPDB (Hermoso et al., 2016a; McClelland et al., 2017; Zeebe and Wolf-Gladrow, 2001). We assume that the DIC species and their respective isotopic compositions ( $\delta^{13}\text{C}$  and  $\delta^{18}\text{O}$ ) were in isotopic equilibrium with  $\text{H}_2\text{O}$  and other ions in the seawater when the experiment commenced. The magnitude of isotopic offset from calculated inorganic calcite values (Table S2, Supplementary Material), deemed the vital effect, were derived as  $\delta^{13}\text{C}_{\text{Coccolith}} - \delta^{13}\text{C}_{\text{Inorganic Calcite}}$  and  $\delta^{18}\text{O}_{\text{Coccolith}} - \delta^{18}\text{O}_{\text{Inorganic Calcite}}$  (Fig. 3). The  $\Delta^{13}\text{C}_{\text{Coccolith}}$  and  $\Delta^{18}\text{O}_{\text{Coccolith}}$  values aligned with previous studies (see Results: Supplementary Material).

### 3.4. Species-specific coccolith vital effects

A crucial reference point to infer species-specific offsets is the isotopic composition of inorganic calcite, which is affected by both equilibrium and thermodynamic fractionation effects due to pH. At a given temperature, the  $\delta^{13}\text{C}$  and  $\delta^{18}\text{O}$  values of inorganic calcite are determined by the speciation of carbon species in the DIC according to the pH (Zeebe, 1999). With increasing pH, the  $\delta^{18}\text{O}$  value of the inorganic calcite will become more depleted due to the increasing proportion of isotopically depleted  $\text{CO}_3^{2-}$  ions, referred to as the “carbonate ion effect” (Zeebe, 1999; Ziveri et al., 2012).

Although the  $\delta^{13}\text{C}$  of carbonate species varies within the carbonate system, with the  $\delta^{13}\text{C}$  of  $\text{CO}_2$  being (-9) ‰ more depleted, and  $\delta^{13}\text{C}$  of  $\text{CO}_3^{2-}$  (-2) ‰ more depleted compared to that of  $\text{HCO}_3^-$  (Zeebe and Wolf-Gladrow, 2001), the  $\delta^{13}\text{C}$  of the calculated inorganic calcite should exhibit no change at equilibrium. This is because if the inorganic calcite is precipitated with all DIC species, the  $\delta^{13}\text{C}$  of the inorganic calcite should only show a consistent 1‰ enrichment in the solid irrespective of the pH (Romanek et al., 1992).

*G. huxleyi* displays slightly positive  $\Delta^{13}\text{C}_{\text{Coccolith}}$  values (up to (+)2 ‰ enrichment than  $\delta^{13}\text{C}_{\text{Inorganic Calcite}}$ ) when  $\text{CO}_2$  levels are below  $\sim 17 \mu\text{mol kg}^{-1}$  (below pH 8.1; Fig. 3a). However, when  $\text{CO}_2$  levels go above this threshold, *G. huxleyi* exhibits negative vital effects in  $\Delta^{13}\text{C}_{\text{Coccolith}}$  (Fig. 3a). A similar shift in vital effects is observed in *G. oceanica* at  $17 \mu\text{mol kg}^{-1} \text{CO}_2$ . However, *G. oceanica* shows near-inorganic  $\Delta^{13}\text{C}_{\text{Coccolith}}$  values ( $< (-)2$  ‰ depletion than  $\delta^{13}\text{C}_{\text{Inorganic Calcite}}$ ) at  $\text{CO}_2$  levels below  $17 \mu\text{mol kg}^{-1}$  in  $\Delta^{13}\text{C}_{\text{Coccolith}}$ . Moreover,  $\Delta^{13}\text{C}_{\text{Coccolith}}$  values for *G. oceanica* above  $17 \mu\text{mol kg}^{-1} \text{CO}_2$  are more negative compared to *G. huxleyi*. These observations suggest that both *G. huxleyi* and *G. oceanica* exhibit near-inorganic vital effects below  $\sim 17 \mu\text{mol kg}^{-1} \text{CO}_2$  (corresponding to a pH of 8.1), while above this  $\text{CO}_2$  concentration, *G. huxleyi* and *G. oceanica* display negative vital effects in  $\Delta^{13}\text{C}_{\text{Coccolith}}$ .  $\Delta^{18}\text{O}_{\text{Coccolith}}$  values exhibit similar trends to  $\Delta^{13}\text{C}_{\text{Coccolith}}$  (Fig. 3b). When compared to the inorganic calcite by Kim and O’Neil (1997), *G. huxleyi* and *G. oceanica* display positive vital effects in  $\Delta^{18}\text{O}_{\text{Coccolith}}$  values below  $\sim 17 \mu\text{mol kg}^{-1} \text{CO}_2$ . While above this threshold, *G. huxleyi* exhibits near-inorganic  $\Delta^{18}\text{O}_{\text{Coccolith}}$  values, and *G. oceanica* exhibits negative  $\Delta^{18}\text{O}_{\text{Coccolith}}$  values.

Vital effects in  $\Delta^{13}\text{C}_{\text{Coccolith}}$  of *C. braarudii* and *C. leptopus* show a consistent depletion of  $\sim 4$  ‰ compared to the inorganic value, except when  $\text{CO}_2$  falls below  $10 \mu\text{mol kg}^{-1}$ , at which point these species display large negative vital effects (Fig. 3a). Regarding  $\Delta^{18}\text{O}_{\text{Coccolith}}$ , *C. braarudii* only exhibits minor deviations from the inorganic values, while *C. leptopus* consistently departs from the inorganic value by a constant offset (Fig. 3b). Finally, *C. carterae* demonstrates that  $\Delta^{13}\text{C}_{\text{Coccolith}}$  values become progressively depleted as  $\text{CO}_2$  concentrations rise (due to lowering pH), while  $\Delta^{18}\text{O}_{\text{Coccolith}}$  values consistently exhibit negative vital effects under all  $\text{CO}_2$  and/or pH conditions, similar to *C. leptopus*.

## 4. Discussion

### 4.1. Growth rate: effect of species-specific $[\text{CO}_2]$ and/or pH optima

We found distinct growth rate optima ( $\mu_{\text{opt}}$ ) for  $\text{CO}_2$  and/or pH among various coccolithophore species. Notably, *C. braarudii* and *C. leptopus* exhibited  $\mu_{\text{opt}}$  values at  $21.05$  (pH 8.02) and  $16.3 \mu\text{mol kg}^{-1} \text{CO}_2$  (pH 8.1) respectively (Fig. 1). *C. carterae* demonstrated a  $\mu_{\text{opt}}$  value at  $13.5 \mu\text{mol kg}^{-1} \text{CO}_2$  (pH 8.22), while *G. oceanica* displayed a  $\mu_{\text{opt}}$  value at  $3.5 \mu\text{mol kg}^{-1} \text{CO}_2$  (pH 8.7). *G. huxleyi* did not exhibit an upper

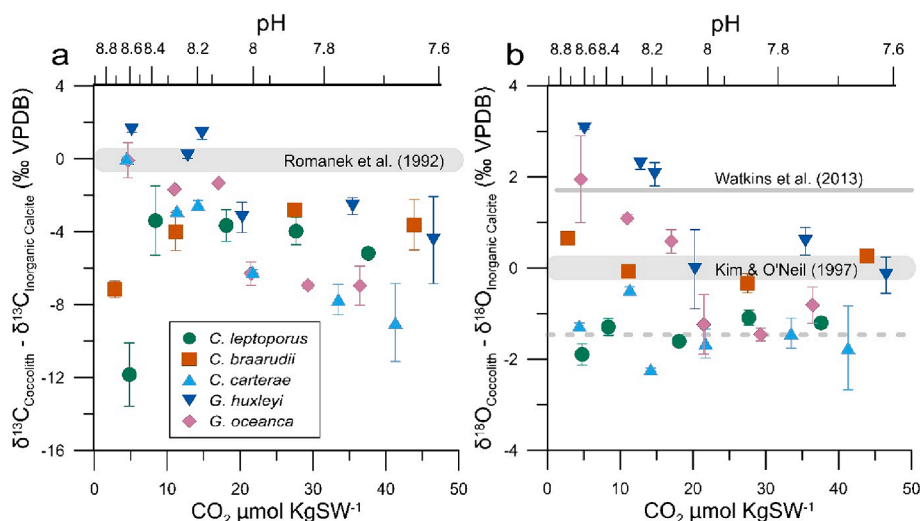


**Fig. 3.** (a) Vital effects in  $\Delta^{13}\text{C}_{\text{Coccolith}}$  ( $\delta^{13}\text{C}_{\text{Coccolith}} - \delta^{13}\text{C}_{\text{Inorganic Calcite}}$ ). 0 ‰ (grey line) signifies  $\delta^{13}\text{C}_{\text{Inorganic Calcite}}$  based on Romanek et al. (1992). (b) Vital effects in  $\Delta^{18}\text{O}_{\text{Coccolith}}$  ( $\delta^{18}\text{O}_{\text{Coccolith}} - \delta^{18}\text{O}_{\text{Inorganic Calcite}}$ ) using  $\delta^{18}\text{O}$  of pH-corrected inorganic calcite. The  $\Delta^{18}\text{O}_{\text{Coccolith}}$  values for *C. carterae* and *C. leptopus* can be compared to the dashed line due to their elevated intracellular pH causing depleted  $\Delta^{18}\text{O}_{\text{Coccolith}}$  values. The grey line at 0 ‰ signifies  $\delta^{18}\text{O}_{\text{Inorganic Calcite}}$  based on Kim and O’Neil (1997), and at 1.79 ‰ based on (Watkins et al., 2013). The thickness of grey lines accounts for the standard deviation in the isotopic composition of the inorganic calcite. Each data point signifies an average of  $\geq 3$  biological replicates, each with  $\geq 3$  replicate measurements.

$\mu_{\text{opt}}$  limit ( $< 5 \mu\text{mol kg}^{-1}$ ,  $\text{pH} > 8.8$ ). A growth optimum likely sits at the intersection of  $\text{H}^+$ -induced growth inhibition and  $\text{CO}_2$  fertilisation at low pH, and alleviation of  $\text{H}^+$ -related inhibition, high pH-related cellular stress, and  $\text{CO}_2$  limitation at high pH. Moreover, species-specific optima exist due to the contrasting physiologies and carbon requirements of the species studied here.

The  $\mu_{\text{opt}}$  values at high  $\text{CO}_2$  (and low pH), for larger-sized, heavily calcifying species such as *C. braarudii*, and *C. leptoporus* is due to their high carbon demand (see Table S1 for species-specific PIC and POC quotas, Supplementary Material). Moreover, the ancestral lineages to these species existed in more acidic,  $\text{CO}_2$ -rich waters during the Paleogene (Agnini et al., 2014; Ridgwell, 2005; Young, 1998). A significant growth rate decline in both *C. braarudii* and *C. leptoporus* is observed below  $10 \mu\text{mol kg}^{-1} [\text{CO}_2]$ , when approaching the lower limit of their optimum curve (Fig. 1). The decline suggests a  $\text{CO}_2$  limitation at lower  $[\text{CO}_2]$  (Bach et al., 2013, 2011). Signs of carbon starvation are also evident in the coccolith malformations of *C. braarudii* under low  $\text{CO}_2$  conditions (Fig. S6, Supplementary Material). The declining growth rates suggests that these species rely predominantly on passive  $\text{CO}_2$  diffusion as their carbon source and are less able to use  $\text{HCO}_3^-$ , which is abundant at the higher pH conditions (Zeebe and Wolf-Gladrow, 2001). At lower  $\text{CO}_2$  levels, diffusive and active carbon uptake may be insufficient or have too low affinity to meet the carbon demands of these two species.

The notion of active carbon uptake has been primarily explored in the context of *G. huxleyi* (Mackinder et al., 2010; Rokitta and Rost, 2012; Sikes et al., 1980). Therefore, it is plausible that the active carbon uptake capabilities might explain the absence of a lower limit for a growth optimum for *G. huxleyi*, which also has a comparably low carbon demand due to its small size and low PIC quotas (Table S1). Similar mechanisms probably exist in the case of the small sized and lightly calcifying *G. oceanica*, as it exhibits a similar trend to *G. huxleyi* in its growth rates (Fig. 1). *G. huxleyi* exhibits high affinity for  $\text{CO}_2$  and/or an effective active carbon uptake mechanism as suggested by the reported half-saturation rate ( $K_c$ ) for growth at  $1.7 \mu\text{mol kg}^{-1} \text{CO}_2$  (Feng et al., 2017), which aligns with its  $\mu_{\text{opt}}$  value at low  $\text{CO}_2$  concentrations. This is noteworthy, given the high half-saturation rates for RuBisCO in *G. huxleyi*, reportedly at  $39 - 41 \mu\text{mol kg}^{-1} \text{CO}_2$  (Heureux, 2016; note the difference between half-saturation rates for growth and RuBisCO). These findings further support the presence of an active carbon concentrating mechanism (CCM) in *G. huxleyi*, particularly under low  $\text{CO}_2$  conditions (Kottmeier et al., 2014; Reinfelder, 2010; Zhang et al., 2021). Given the predominant focus on the active carbon uptake mechanisms in *G. huxleyi*, it is important to determine the extent of this mechanism in other species, particularly those which exhibit  $\mu_{\text{opt}}$  values at high  $\text{CO}_2$  concentrations due to their larger size and/or higher calcification requirements as highlighted in previous studies (Bach et al., 2015; Daniels et al., 2014).

The  $\mu_{\text{opt}}$  value for *C. carterae* at a relatively higher  $\text{CO}_2$  concentration is possibly due to its large cell size, despite being the lowest PIC:POC species (Table S1, Supplementary Material).  $\mu_{\text{opt}}$  values at a higher  $\text{CO}_2$  concentration may be due to the large internal carbon pool of *C. carterae* (also *C. braarudii* and *C. leptoporus*), which requires higher carbon fluxes into the cell for its replenishment or due to their higher internal pH buffering capacities. A decrease in coccosphere size for *C. carterae* was observed with decreasing  $[\text{CO}_2]$ /increasing pH, resulting in a  $\sim 60\%$  increase in Surface Area to Volume (SA:V) ratio (Fig. S2, Supplementary Material). An increase in the SA:V ratio may potentially aid  $\text{CO}_2$  diffusion into the cell under reduced  $\text{CO}_2$  availability. Alternatively, cell size may increase under low pH due to elevated  $[\text{H}^+]$ -driven reduced cellular division rates (inferred from reduced growth rates at low pH in Fig. 1). Nonetheless, the flexibility in cell size and the plateau in growth rates at a wide pH range (pH 8–8.7) can be a trait related to the dynamic coastal habitat of *C. carterae* (Houdan et al., 2004).

Increased carbon supply at higher  $\text{CO}_2$  concentrations has been shown to enhance growth due to its fertilizing effect on phytoplankton,

as the enzyme RuBisCO utilizes  $\text{CO}_2$  for carbon fixation (Fiorini et al., 2011; Iglesias-Rodriguez et al., 2008). This phenomenon has been previously demonstrated in the case of *C. braarudii* (Halloran et al., 2008; Langer et al., 2006), which is consistent with our findings of  $\mu_{\text{opt}}$  values at high  $\text{CO}_2$  concentrations for the same species.

Our study reveals a consistent decline in growth rates for all species, especially at  $[\text{CO}_2]$  greater than  $30 \mu\text{mol kg}^{-1}$  (below pH 7.9). This observation coincides with increased malformation in the coccolith calcite (Fig. S6, Supplementary Material) suggesting the inhibitory effect of increased  $[\text{H}^+]$  associated with decreasing pH is experienced universally (Bach et al., 2015; Suffrian et al., 2011; Taylor et al., 2011). In terms of pH sensitivity, the inhibitory effect of pH in *G. huxleyi* and *G. oceanica* is observed as a continuous decline in growth rates starting from pH 8.4 and progressing to lower pH values. However, the inhibitory effect of low pH on the growth rates of *C. braarudii*, *C. leptoporus* and *C. carterae* is observed only at pH levels below 7.9. This implies that the larger species (*C. braarudii*, *C. leptoporus* and *C. carterae*) display a stronger threshold towards sensitivity to declining pH which may be attributed to their stronger intracellular pH buffering capacity due to their comparatively large size and small SA:V ratio (Table S1).  $\text{H}^+$  efflux during calcification through membrane channels has been previously documented as the mechanism responsible for pH homeostasis in *C. braarudii* (Kottmeier et al., 2022; Taylor et al., 2011). It is plausible that this mechanism is also operative in *C. leptoporus* and *C. carterae*, contributing to their higher tolerance to variable pH.

#### 4.2. The relationship between vital effects and carbon demand to supply ratio

Species-specific growth rates at varying  $\text{CO}_2$  and pH levels allows the investigation of vital effects to the carbon demand to supply ratio (represented as  $\mu/\text{CO}_2$ ) and often used to describe the sensitivity of carbon isotopic fractionation into organic matter (e.g., Keller and Morel, 1999). While previous research has examined the relationship between  $\mu/\text{CO}_2$  and vital effects in coccolith calcite (e.g., Hermoso, 2015) and isotopic fractionation in organic matter (e.g., Tchernov et al., 2014), studies rarely address both the organic and inorganic systems simultaneously.

Although the parameter  $\mu/\text{CO}_2$ , as a measure of the carbon demand versus supply, may not incorporate factors such as the additional carbon demand imposed by a calcifying cell for biomineralisation, or carbon supply through active  $\text{HCO}_3^-$  uptake, it does offer a framework for interpretation (Hermoso et al., 2016b). This significance is magnified as the portion of carbon supply via active  $\text{HCO}_3^-$  uptake has only been quantified in one coccolithophore species (Kottmeier et al., 2014; Kottmeier et al., 2016a). According to Kottmeier et al. (2014), *G. huxleyi* used  $>90\%$   $\text{CO}_2$  below pH of 8.1 ( $[\text{CO}_2]$  greater than  $17 \mu\text{mol kg}^{-1}$  for this study) and the proportion of active  $\text{HCO}_3^-$  uptake progressively increased above pH 8.1, with  $\sim 55\%$   $\text{HCO}_3^-$  at pH 8.7. The current study did not measure calcification rates so these cannot be factored into the carbon demand calculation. SA:V ratio is included to get a better estimate of carbon demand through organic carbon fixation and diffusive supply of  $\text{CO}_2$ , especially with changing cell sizes. In this study, SA:V calculations were based on coccosphere diameters rather than naked cell sizes, as measuring the latter resulted in higher inaccuracies.

Vital effects in Fig. 3 suggest that large-sized and heavily calcifying species such as *C. braarudii* and *C. leptoporus* that show  $\mu_{\text{opt}}$  values at high  $\text{CO}_2$  concentrations, show a consistent depletion of  $\sim (-)4\%$  from inorganic calcite under most scenarios, and only exhibit significant offsets in  $\Delta^{13}\text{C}_{\text{Coccolith}}$  under the lowest  $\text{CO}_2$  concentrations. Small-sized and lightly calcifying species such as *G. huxleyi* and *G. oceanica* that show a  $\mu_{\text{opt}}$  value at low  $\text{CO}_2$  concentrations, show a shift towards more depleted values at  $17 \mu\text{mol kg}^{-1} \text{CO}_2$  but display a constant offset from each other across the conditions. Finally, *C. carterae* that exhibit  $\mu_{\text{opt}}$  values at intermediate  $\text{CO}_2$  concentrations, display progressively depleted  $\Delta^{13}\text{C}_{\text{Coccolith}}$  values with increasing  $\text{CO}_2$  while  $\Delta^{18}\text{O}_{\text{Coccolith}}$

values show minimal changes. In the following section, we investigate the relationship between vital effects and carbon demand to supply ratio in these three groups, and provide insights into the observed trends in  $\Delta^{13}\text{C}_{\text{Coccolith}}$ ,  $\Delta^{18}\text{O}_{\text{Coccolith}}$ , and  $\Delta^{13}\text{C}_{\text{ORG}}$  across varying growth rates,  $\text{CO}_2$ , and pH levels.

4.2.1. Long carbon residence times in *C. braarudii* and *C. leptoporus* allow isotopic equilibration of their internal pool: vital effects emerge during lowest carbon supply and high carbon demand

Above  $[\text{CO}_2]$  of  $10 \mu\text{mol kg}^{-1}$ , growth rates decrease at high  $\text{CO}_2$ , and coccoliths show malformations with increasing  $\text{CO}_2$  (Fig. S6, Supplementary Material) for *C. braarudii* and *C. leptoporus*. Moreover, their  $\Delta^{13}\text{C}_{\text{Coccolith}}$  values show a consistent offset from the  $\delta^{13}\text{C}$  of inorganic calcite (grey line, Fig. 4a), with minor variations in isotopic values with increasing  $\text{CO}_2$  (Fig. 4a), and minimal changes with  $\mu/\text{CO}_2$  ( $[\text{CO}_2] > 10 \mu\text{mol kg}^{-1}$ ; Fig. 4c). Similar offsets at high  $[\text{CO}_2]$  have been reported previously (Hermoso, 2015; Wilkes et al., 2018). At  $[\text{CO}_2]$  above  $10 \mu\text{mol kg}^{-1}$ ,  $\Delta^{13}\text{C}_{\text{ORG}}$  values become more depleted with increasing  $\text{CO}_2$  and decreasing growth rates (Fig. 2c, 4b). This observation is consistent with previous studies that report a depletion in  $\Delta^{13}\text{C}_{\text{ORG}}$  values with increasing diffusive  $\text{CO}_2$  supply due to increasing ambient  $\text{CO}_2$  concentration (e.g., Burkhardt et al., 1999a).

Regarding  $\Delta^{18}\text{O}_{\text{Coccolith}}$  values, *C. braarudii* exhibits minor offsets from inorganic calcite, while  $\Delta^{18}\text{O}_{\text{Coccolith}}$  values for *C. leptoporus* show a consistent offset towards depleted values from the inorganic value under all  $\text{CO}_2$  conditions (Fig. 2b, 3b). The lack of changes in  $\Delta^{18}\text{O}_{\text{Coccolith}}$  with

$\mu/\text{CO}_2$  suggest that carbon residence times are long enough to allow isotopic equilibration of the oxygen isotopes with intracellular  $\text{H}_2\text{O}$  (Fig. 4d). The offset in  $\Delta^{18}\text{O}_{\text{Coccolith}}$  towards depleted values in *C. leptoporus* can be attributed to the pH of the calcifying fluid within the coccolith vesicle (described hereafter as intracellular pH) being higher than the ambient pH, as reported previously (Liu et al., 2021). Specifically, under high intracellular pH,  $\Delta^{18}\text{O}_{\text{Coccolith}}$  becomes depleted due to the increased proportion of the (isotopically depleted)  $\text{CO}_3^{2-}$  ions. Although intracellular pH may increase proportionally with ambient pH (Suffrian et al., 2011), active  $\text{Ca}^{2+}/\text{H}^+$  exchangers can raise the pH of the calcifying fluid to increase the calcite saturation state, therefore, affecting the  $\text{CO}_3^{2-}/\text{HCO}_3^-$  ratio (Anning et al., 1996; Chen et al., 2018; Mackinder et al., 2010). It is worth noting that the  $\delta^{18}\text{O}$  value of  $\text{CO}_3^{2-}$  itself becomes more depleted with rising pH (Zeebe, 1999). Similar mechanisms of elevating intracellular pH to promote calcification have been observed in corals (Venn et al., 2011).

Below  $[\text{CO}_2]$  of  $10 \mu\text{mol kg}^{-1}$ ,  $\Delta^{13}\text{C}_{\text{Coccolith}}$ ,  $\Delta^{13}\text{C}_{\text{ORG}}$ , and growth rates for *C. braarudii* and *C. leptoporus* show a consistent decline (Fig. 1, 2a,c, 4a,b). This observation points to a unifying factor driving the concurrent isotopic depletion in the calcite and organic matter, which is a consequence of alterations in the isotopic composition of the shared internal pool (Fig. 2a,c, 4b). Under  $\text{CO}_2$ -limiting conditions, where growth rates are  $\text{CO}_2$ -limited and imply a diminished internal carbon pool, a strong  $\text{CO}_2$  gradient is established between the highly utilised (and therefore low concentration) intracellular carbon pool and the ambient seawater that facilitates high rates of passive diffusion of

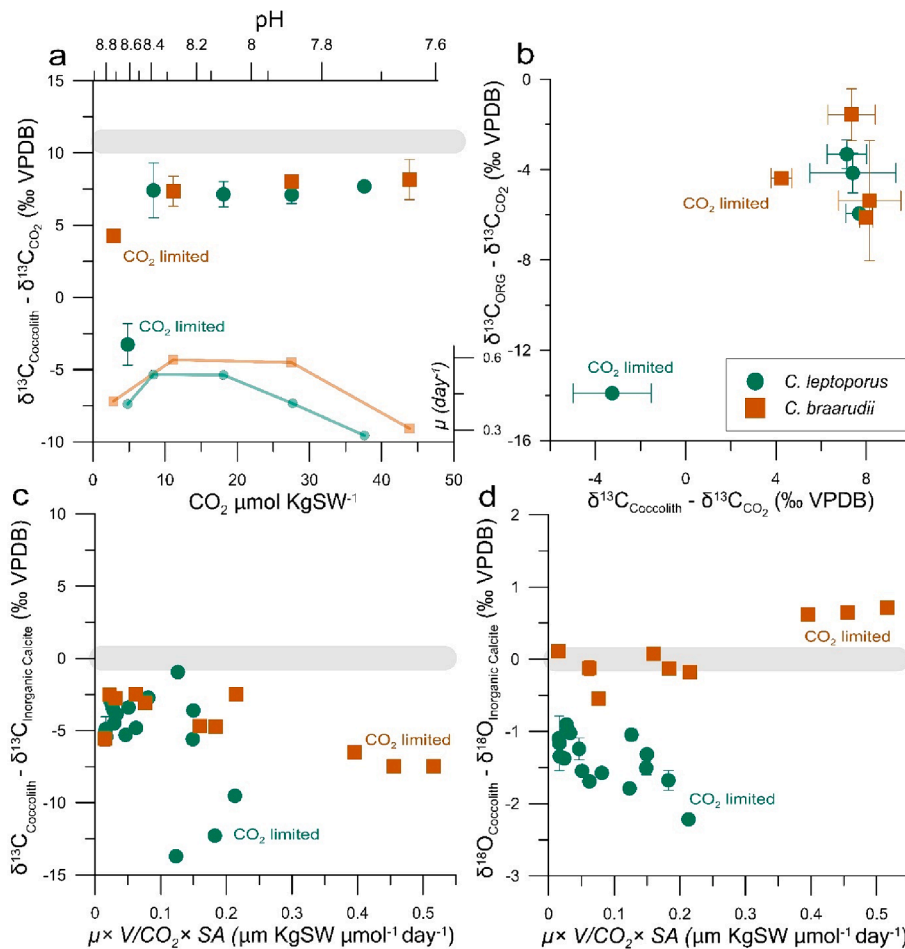


Fig. 4. (a)  $\delta^{13}\text{C}_{\text{Coccolith}} - \delta^{13}\text{C}_{\text{CO}_2}$  for *C. braarudii* (■) and *C. leptoporus* (●) with growth rate ( $\mu$ ,  $\text{day}^{-1}$ ) plotted as a subset. Grey line denotes inorganic calcite. (b)  $\Delta^{13}\text{C}_{\text{Coccolith}}$  vs.  $\Delta^{13}\text{C}_{\text{ORG}}$  (c)  $\delta^{13}\text{C}_{\text{Coccolith}} - \delta^{13}\text{C}_{\text{Inorganic Calcite}}$  vs.  $\mu \times V/\text{CO}_2 \times \text{SA}$  (d)  $\delta^{18}\text{O}_{\text{Coccolith}} - \delta^{18}\text{O}_{\text{Inorganic Calcite}}$  vs.  $\mu \times V/\text{CO}_2 \times \text{SA}$ . The line thickness at 0 ‰ accounts for the standard deviation in the isotopic composition of the inorganic calcite. Note that in (a) and (b), the replicates are averaged, while in (c) and (d), they are not averaged.  $\delta^{13}\text{C}_{\text{ORG}} - \delta^{13}\text{C}_{\text{DIC}}$  vs  $\mu \times V/\text{CO}_2 \times \text{SA}$  can be found in the Supplementary Material (Fig. S5).

isotopically depleted CO<sub>2</sub> (~9 ‰ depleted compared to DIC, for δ<sup>13</sup>C) into the coccolithophore cell. Within the carbon depleted internal pool, there is very little carbon for isotopic exchange, such that the carbon isotopes of the internal pool tend towards that of the carbon supply. The calcite and organic matter then reflect the CO<sub>2</sub>-induced depletion in isotopic values of the starved carbon pool, which has allowed no carbon isotopic equilibration as both calcification and organic matter fixation draw carbon from the same intracellular carbon pool (Holtz et al., 2017; Kaplan and Reinhold, 2003; Tchernov et al., 2001). A strong coupling between Δ<sup>13</sup>C<sub>Coccolith</sub> and Δ<sup>13</sup>C<sub>ORG</sub> suggest that the primary substrate for the internal carbon pool is CO<sub>2</sub> (Hermoso, 2015) and that a mechanistic relationship exists between the cell cycle and calcification, which has previously been suggested for *C. braarudii* (Walker et al., 2018).

The internal carbon pool represents carbon dissolved in a water

media such that there are sufficient oxygen atoms available from H<sub>2</sub>O to equilibrate the oxygen isotopes given sufficient residence time, which dilutes the heavy oxygen isotopic signal of the diffusing CO<sub>2</sub> (Hermoso et al., 2016). An aggravated CO<sub>2</sub> gradient stems from the extremely high carbon demands (μ<sub>opt</sub> at high CO<sub>2</sub> concentrations, high PIC, large cell size) for these species and severely starved intracellular carbon concentrations at low [CO<sub>2</sub>]. Moreover, passive CO<sub>2</sub> diffusion can be enhanced under low [CO<sub>2</sub>] through H<sup>+</sup> efflux to maintain pH homeostasis during calcification or during Ca<sup>2+</sup>/H<sup>+</sup> exchange (Mackinder et al., 2010; Taylor et al., 2011).

The difference in Δ<sup>18</sup>O<sub>Coccolith</sub> offsets for *C. braarudii* and *C. leptopus* suggest contrasting mechanisms for intracellular pool equilibration, where *C. braarudii* possesses a large intracellular pool with long carbon residence times, allowing isotopic equilibration and μ<sub>opt</sub>

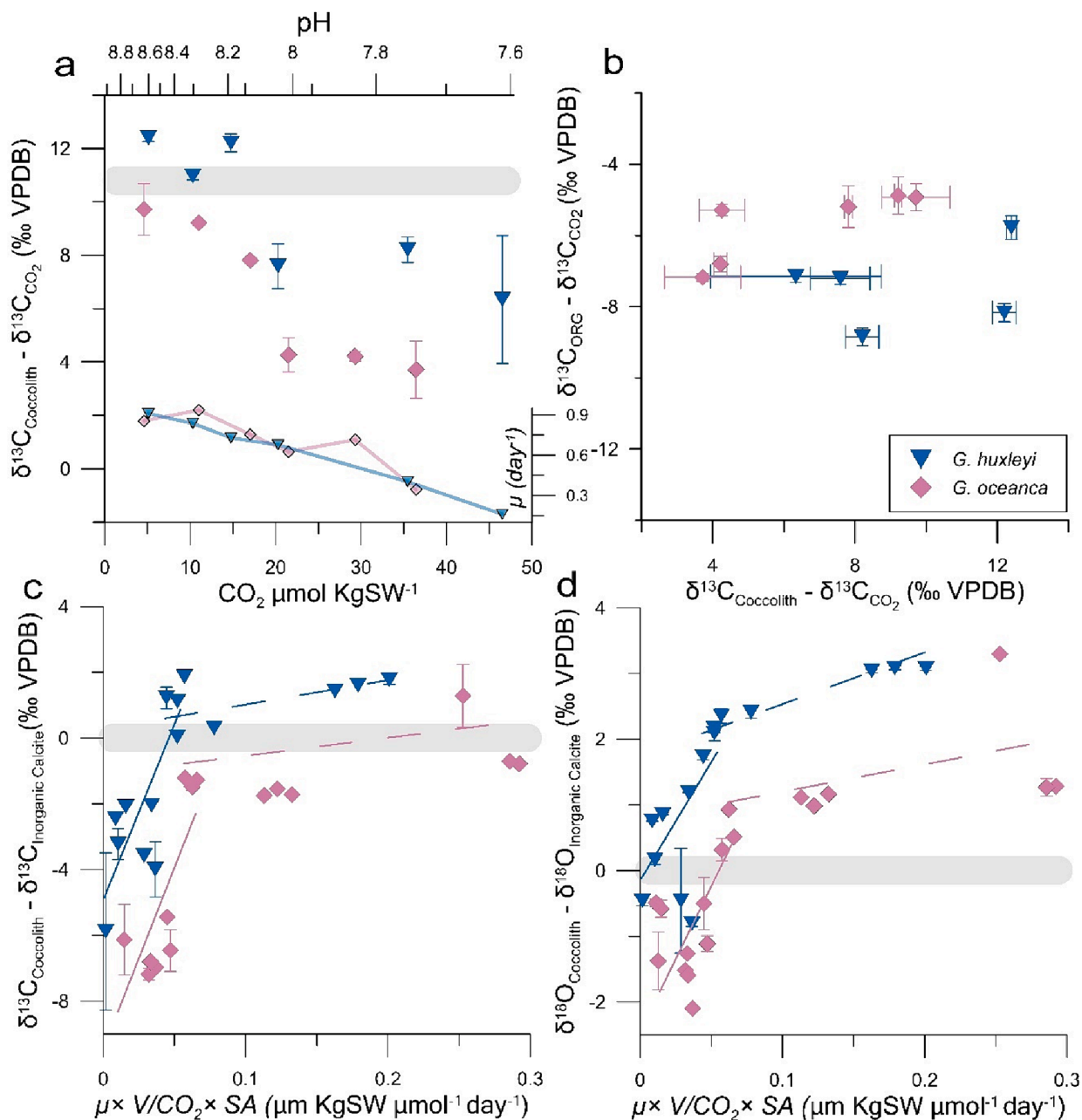


**Fig. 5.** (a)  $\delta^{13}\text{C}_{\text{Coccolith}} - \delta^{13}\text{C}_{\text{CO}_2}$  for *G. huxleyi* (▼) and *G. oceanica* (◆) with growth rate ( $\mu$ , day<sup>-1</sup>) plotted as a subset. Grey line denotes inorganic calcite. (b)  $\Delta^{13}\text{C}_{\text{Coccolith}}$  vs.  $\Delta^{13}\text{C}_{\text{ORG}}$  (c)  $\delta^{13}\text{C}_{\text{Coccolith}} - \delta^{13}\text{C}_{\text{Inorganic Calcite}}$  vs.  $\mu \times V/\text{CO}_2 \times \text{SA}$  (d)  $\delta^{18}\text{O}_{\text{Coccolith}} - \delta^{18}\text{O}_{\text{Inorganic Calcite}}$  vs.  $\mu \times V/\text{CO}_2 \times \text{SA}$ . The line thickness at 0 ‰ accounts for the standard deviation in the isotopic composition of the inorganic calcite. Note that in (a) and (b), the replicates are averaged, while in (c) and (d), they are not averaged.  $\delta^{13}\text{C}_{\text{ORG}} - \delta^{13}\text{C}_{\text{DIC}}$  vs  $\mu \times V/\text{CO}_2 \times \text{SA}$  can be found in the Supplementary Material (Fig. S5).

values at higher CO<sub>2</sub> concentrations. Moreover,  $\Delta^{18}\text{O}_{\text{Coccolith}}$  values similar to those of inorganic calcite suggest high intracellular pH buffering capacity in *C. braarudii* (Fig. 2b, 3b). Whereas *C. leptoporus* possesses a smaller intracellular carbon pool (compared to *C. braarudii*), which is more susceptible to depletion, but higher intracellular pH and long residence times for carbon causing an isotopic offset in  $\Delta^{18}\text{O}_{\text{Coccolith}}$  values and  $\mu_{\text{opt}}$  values at higher CO<sub>2</sub> concentrations. The size of the internal carbon pool can be said to be proportional to the size of the cell (Fig. S2). Moreover, the contrasting size of their intracellular carbon pool is marked by the magnitude of isotopic change under CO<sub>2</sub>-limiting conditions where *C. braarudii* exhibits small offsets in  $\delta^{13}\text{C}$  due to a large intracellular carbon pool but *C. leptoporus* displays large depletion in  $\delta^{13}\text{C}$  due to a comparatively smaller internal pool.

Observations reported here are unlikely to be caused by hydroxylation/hydration of CO<sub>2</sub> to HCO<sub>3</sub><sup>-</sup> as changes in  $\Delta^{18}\text{O}_{\text{Coccolith}}$  values with changing CO<sub>2</sub> are negligible (Fig. 2b, 3b, 4d). Moreover, the depletion in  $\Delta^{13}\text{C}_{\text{ORG}}$  as observed at CO<sub>2</sub> below 10  $\mu\text{mol kg}^{-1}$  should not occur during hydration/hydroxylation of CO<sub>2</sub> into HCO<sub>3</sub><sup>-</sup> because CO<sub>2</sub> serves as the primary substrate for RuBisCO and therefore should not be affected by hydration/hydroxylation reactions. Also, the likely presence of carbonic anhydrase in coccolithophores would catalyse this reaction (Reinfelder, 2010).

#### 4.2.2. Vital effects for *G. huxleyi* and *G. oceanica* show greatest change during low carbon demand and high carbon supply due to the short carbon residence times in their internal carbon pools.

The isotopic shift in  $\Delta^{13}\text{C}_{\text{Coccolith}}$  values for *G. huxleyi* and *G. oceanica* at  $\sim 17 \mu\text{mol kg}^{-1}$  (pH 8.1) is caused by changes in the mode of carbon uptake (Kottmeier et al., 2014). CO<sub>2</sub> diffusion driven carbon uptake is prominent at high [CO<sub>2</sub>], causing isotopic depletion in the  $\delta^{13}\text{C}$  of the carbon pool, while active uptake of isotopically heavy ( $\delta^{13}\text{C}$ ) HCO<sub>3</sub><sup>-</sup> brings the pool closer to inorganic values at low [CO<sub>2</sub>] (Fig. 5a). Active carbon uptake is also evident as growth rates are not limited under low CO<sub>2</sub> conditions. Indeed, the best growth conditions for these species appear to be at low CO<sub>2</sub> (Fig. 1; 5a-inset). Alternatively, heavier  $\Delta^{13}\text{C}_{\text{Coccolith}}$  values at low CO<sub>2</sub>/high pH can also be attributed to preferential leakage of lighter CO<sub>2</sub> from the internal carbon pool. CO<sub>2</sub> leakage was previously suggested to be prominent in *G. huxleyi* at low [CO<sub>2</sub>] (Rost et al., 2006). Under low CO<sub>2</sub>, the intracellular carbon pool has a higher carbon concentration than ambient seawater, causing CO<sub>2</sub> leakage, while at high CO<sub>2</sub> (>17  $\mu\text{mol kg}^{-1}$ , pH < 8.1), diffusion of lighter CO<sub>2</sub> into the cell causes isotopic depletion of the intracellular carbon pool, and consequently, the coccolith calcite. This indicates that the intracellular carbon concentration in these species is  $\geq 17 \mu\text{mol kg}^{-1}$  (Liu et al., 2021).

Although shifts in carbon uptake mechanism have been documented through  $\Delta^{13}\text{C}_{\text{ORG}}$  (as  $\mathcal{E}_p$ ) at [CO<sub>2</sub>] of  $\sim 13 \mu\text{mol kg}^{-1}$  (Burkhardt et al., 1999b; Keller and Morel, 1999; Laws et al., 1998; Tchernov et al., 2014), in this study, *G. huxleyi* and *G. oceanica* exhibited only minor changes in  $\Delta^{13}\text{C}_{\text{ORG}}$  (Fig. 2c, 5b), suggesting minimal changes in the isotopic fractionation of carbon into the organic matter. Moreover, the  $\Delta^{13}\text{C}_{\text{ORG}}$  values for *G. huxleyi* are significantly more enriched (6–9 ‰) than those reported for *G. huxleyi* RuBisCO previously (11.1 ‰, Boller et al., 2011). These observations can be due to ample carbon supply that is meeting the cell's carbon demand owing to their small size (large SA:V ratio), and active carbon uptake under low CO<sub>2</sub> concentrations (Table S1). Moreover, no changes in Rayleigh fractionation are observed (through minimal changes in  $\Delta^{13}\text{C}_{\text{ORG}}$ ) due to carbon supply being higher than demand under all pH/CO<sub>2</sub> conditions.

The lack of changes in  $\Delta^{13}\text{C}_{\text{ORG}}$  values for *G. huxleyi* and *G. oceanica* in contrast to the observed changes in  $\Delta^{13}\text{C}_{\text{Coccolith}}$  and  $\Delta^{18}\text{O}_{\text{Coccolith}}$  values indicate a short carbon residence time for these species. A short residence time causes calcification and photosynthesis to “see” different carbon pools as if the processes were offset in time and/or space. The small cell size of *G. huxleyi* and *G. oceanica* (compared to other species in this study), corresponds to a small internal carbon pool in these species,

and reduced internal pH buffering capacity. The higher SA:V ratio and fast calcification rates as reported previously (Balch et al., 1993; Daniels et al., 2014) lead to high CO<sub>2</sub> fluxes in and out of the cell, causing short residence times for carbon in the intracellular carbon pool. Alternatively, the lack of changes in  $\Delta^{13}\text{C}_{\text{ORG}}$  values are possible if resource allocation favoured towards photosynthesis rather than calcification. This seems plausible since *G. huxleyi* exhibits evidence towards a decoupling between calcification photosynthesis as it can still grow non-calcified in nature or when calcification is disrupted through calcium limitation in the laboratory (Paasche, 2001; Trimborn et al., 2007).

$\Delta^{13}\text{C}_{\text{Coccolith}}$  and  $\Delta^{18}\text{O}_{\text{Coccolith}}$  values for *G. huxleyi* and *G. oceanica* exhibit kinetic isotopic fractionation as both isotopic systems show depleting isotopic values with increasing diffusive CO<sub>2</sub> supply (Fig. 5c, d). This observation agrees with Hermoso (2015), where it was suggested that the source of carbon for the internal carbon pool in coccolithophores is mainly CO<sub>2</sub>. Moreover, there is a pronounced change in the gradient of  $\Delta^{13}\text{C}_{\text{Coccolith}}$  and  $\Delta^{18}\text{O}_{\text{Coccolith}}$  values with increasing  $\mu/\text{CO}_2$ , illustrated by the line fits in Figure 5c, d. Under conditions of high CO<sub>2</sub>/low pH and reduced growth rates, diffusive (isotopically light) CO<sub>2</sub> appears to imprint a small internal carbon pool, therefore,  $\Delta^{13}\text{C}_{\text{Coccolith}}$  values become depleted in proportion to the excess CO<sub>2</sub> supply (Fig. 5c). As the  $\mu/\text{CO}_2$  ratio increases, the demand for carbon escalates while the diffusive carbon supply diminishes, which results in enriched isotopic values in these species (Fig. 5c,d; Fig. 4 in McClelland et al., 2017).

Diffused CO<sub>2</sub> should experience a more pronounced depletion in  $\delta^{18}\text{O}$  compared to  $\delta^{13}\text{C}$  (Thiagarajan et al., 2011). This is because the mass difference between <sup>16</sup>O-<sup>18</sup>O is larger than that of <sup>12</sup>C-<sup>13</sup>C, leading to greater fractionation between O isotopes (Wanner and Hunkeler, 2019). In contrast, our study exhibits a larger depletion in the  $\Delta^{13}\text{C}_{\text{Coccolith}}$  (depletion of up to  $\sim 6 \text{‰}$  from inorganic values at highest CO<sub>2</sub>, Fig. 5c) compared to the  $\Delta^{18}\text{O}_{\text{Coccolith}}$  (depletion of  $\sim 2 \text{‰}$  from inorganic values at highest CO<sub>2</sub>, Fig. 5d). The smaller magnitude of change in  $\delta^{18}\text{O}$  compared to  $\delta^{13}\text{C}$  could be due to the small size of the internal carbon pool and rapid turnover time (fluxes in and out of the cell) for carbon which allows for larger isotopic shifts in  $\delta^{13}\text{C}$  due to the addition of CO<sub>2</sub>, but a greater abundance of oxygen through H<sub>2</sub>O allows for partial equilibration of  $\delta^{18}\text{O}$  in the intracellular carbon pool.

A departure from the steep gradient between  $\Delta^{13}\text{C}_{\text{Coccolith}}$  and  $\mu/\text{CO}_2$  emerges at high  $\mu/\text{CO}_2$  (Fig. 5c, d), indicating an impact of the active HCO<sub>3</sub><sup>-</sup> uptake as is predicted for photosynthetic fixation (Laws et al., 2002). This observation points to an active carbon supply mechanism within the cell, which could alleviate carbon limitation as suggested in previous studies (Kottmeier et al., 2016b; Zhang et al., 2021). This is consistent with our growth rate optima for *G. huxleyi* and *G. oceanica*, which is at lower CO<sub>2</sub> concentrations compared to other species. Alternatively, a higher intracellular carbon concentration could enhance CO<sub>2</sub> leakage, driving the internal pool isotopically heavy. Distinguishing between active (HCO<sub>3</sub><sup>-</sup> uptake and CA-facilitated inter-conversion of HCO<sub>3</sub><sup>-</sup> and CO<sub>2</sub>, however, remains challenging due to the similarity in resultant isotopic compositions (Uchikawa and Zeebe, 2012; Zeebe and Wolf-Gladrow, 2001), despite evidence for the presence of external carbonic anhydrase in *G. huxleyi* (see for example, Rost et al., 2003; Stojkovic et al., 2013).

It is important to note that *G. oceanica* consistently exhibits more depleted  $\Delta^{13}\text{C}_{\text{Coccolith}}$  and  $\Delta^{18}\text{O}_{\text{Coccolith}}$  values but isotopically enriched  $\Delta^{13}\text{C}_{\text{ORG}}$  values than *G. huxleyi*. Similar offsets between these two species have been previously observed (Hermoso et al., 2016b). Such an effect could be causal, that is, removal of depleted carbon from the intracellular carbon pool into calcite leaves the pool isotopically enriched from which the organic matter draws its carbon. Alternatively, the smaller carbon isotopic fractionation into  $\Delta^{13}\text{C}_{\text{ORG}}$  for *G. oceanica* compared to *G. huxleyi* could imply a smaller internal carbon pool in *G. oceanica*, which is then more susceptible to overprinting from the high diffusive supply rate of CO<sub>2</sub> at low pH and has less CO<sub>2</sub> to lose diffusively at low CO<sub>2</sub> (high pH) due to its larger cell size. However, since the size of

internal carbon pools are proportional to cell size, we suspect a comparatively larger internal pool in *G. oceanica*.

The  $\Delta^{13}\text{C}_{\text{Coccolith}}$  and  $\Delta^{18}\text{O}_{\text{Coccolith}}$  trends observed for *G. huxleyi* and *G. oceanica* in this study could also be a consequence of hydration/hydroxylation related kinetic isotope effects. However, the known presence of carbonic anhydrase negates this hypothesis (Rost et al., 2003). Moreover, the trends in  $\Delta^{13}\text{C}_{\text{Coccolith}}$  and  $\Delta^{18}\text{O}_{\text{Coccolith}}$  show a significant shift in isotopic values at  $\text{CO}_2$  of  $17 \mu\text{mol kg}^{-1}$  (pH 8.1), which cannot be explained by hydration/hydroxylation related kinetic isotope effects. Such a scenario is only possible if hydration/hydroxylation related kinetic isotope effects were taking place in addition to  $\text{CO}_2$  leakage /  $\text{HCO}_3^-$  uptake (as seen through the horizontal lines and enriched/heavy isotopic values in Fig. 3 and 5c,d). Moreover, photosynthetic carbon fixation and calcification would need to have distinct intracellular carbon pools such that carbonic anhydrase and Rayleigh fractionation due to RuBisCO do not affect the carbon pool allocated to calcification only.

Such a mechanism could resolve the discrepancy between  $\Delta^{13}\text{C}_{\text{Coccolith}}$  and  $\Delta^{13}\text{C}_{\text{ORG}}$  values.

#### 4.2.3. Carbon vital effects in *C. carterae* are sensitive to changing carbon supply but long carbon residence times alleviate oxygen vital effects

$\Delta^{13}\text{C}_{\text{Coccolith}}$  values in *C. carterae* exhibit a linear trend despite varying growth rates across different  $\text{CO}_2$  concentrations (Fig. 6a). This species lacks a covariation in  $\Delta^{13}\text{C}_{\text{Coccolith}}$  and  $\Delta^{18}\text{O}_{\text{Coccolith}}$  unlike any other species studied here (Fig. 3, 6c,d). Moreover, depletion in the  $\Delta^{13}\text{C}_{\text{Coccolith}}$  ( $R^2 = 0.86$ ) and  $\Delta^{13}\text{C}_{\text{ORG}}$  ( $R^2 = 0.88$ ) linearly correlate with increasing  $[\text{CO}_2]$ , suggesting that organic carbon fixation and calcification in *C. carterae* source their carbon from a shared intracellular carbon pool, with the same change in the carbon pool being reflected in both organic and inorganic carbon reservoirs (Fig. 6b). Such a shared intracellular carbon pool appears to be integral, a concept previously observed (Liu et al., 2021, 2018). The linear relationship also suggests

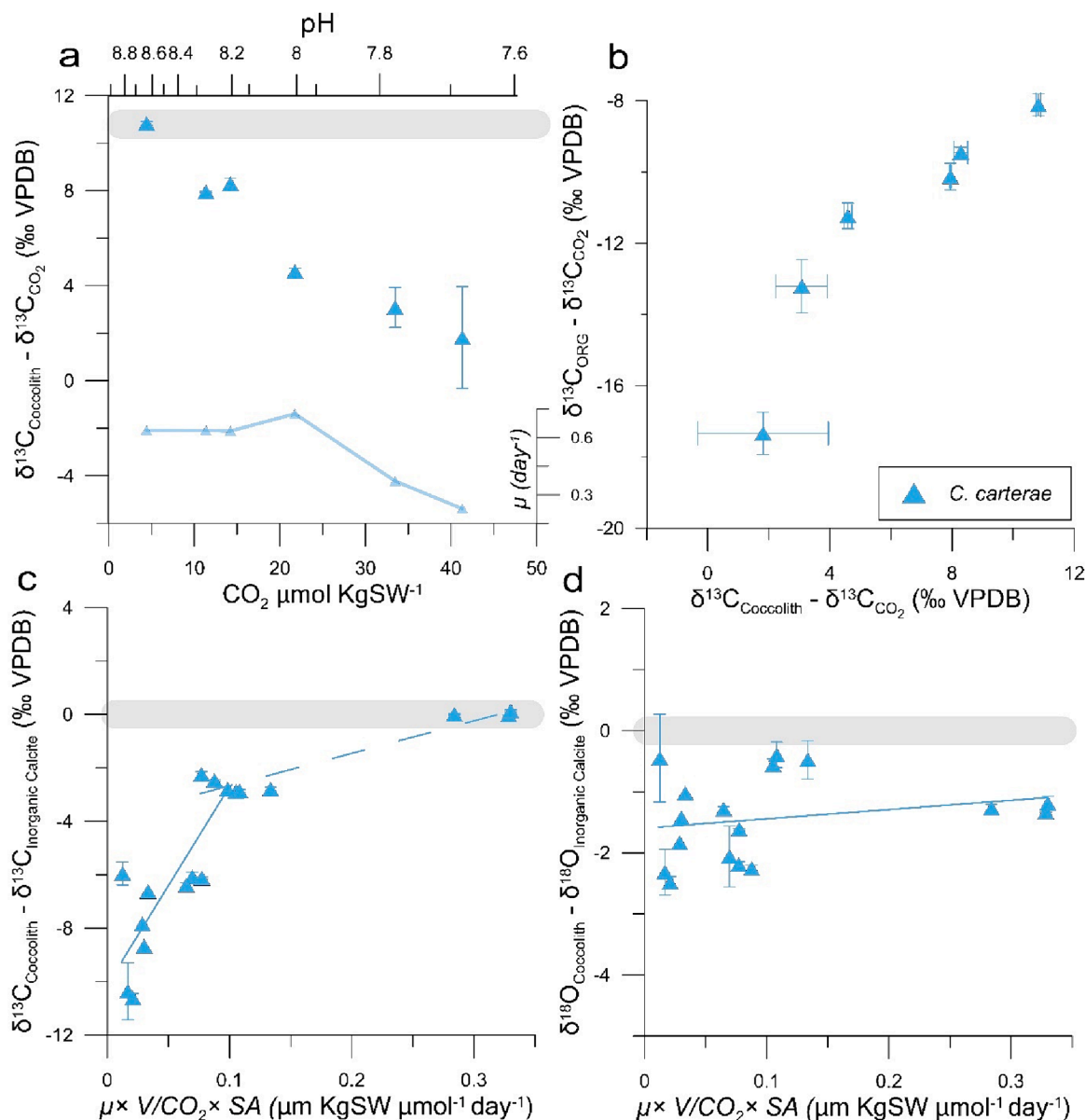


**Fig. 6.** (a)  $\delta^{13}\text{C}_{\text{Coccolith}} - \delta^{13}\text{C}_{\text{CO}_2}$  for *C. carterae* ( $\blacktriangle$ ) with growth rate ( $\mu$ ,  $\text{day}^{-1}$ ) plotted as a subset. Grey line denotes inorganic calcite. (b)  $\Delta^{13}\text{C}_{\text{Coccolith}}$  vs.  $\Delta^{13}\text{C}_{\text{ORG}}$  (c)  $\delta^{13}\text{C}_{\text{Coccolith}} - \delta^{13}\text{C}_{\text{Inorganic Calcite}}$  vs.  $\mu \times V/\text{CO}_2 \times \text{SA}$  (d)  $\delta^{18}\text{O}_{\text{Coccolith}} - \delta^{18}\text{O}_{\text{Inorganic Calcite}}$  vs.  $\mu \times V/\text{CO}_2 \times \text{SA}$ . The line thickness at 0 ‰ accounts for the standard deviation in the isotopic composition of the inorganic calcite. Note that in (a) and (b), the replicates are averaged, while in (c) and (d), they are not averaged.  $\delta^{13}\text{C}_{\text{Coccolith}} - \delta^{13}\text{C}_{\text{DIC}}$  vs  $\mu \times V/\text{CO}_2 \times \text{SA}$  can be found in the Supplementary Material (Fig. S5).  $\delta^{13}\text{C}_{\text{ORG}} - \delta^{13}\text{C}_{\text{DIC}}$  vs  $\mu \times V/\text{CO}_2 \times \text{SA}$  can be found in the Supplementary Material (Fig. S5).

high sensitivity to CO<sub>2</sub> concentrations across high growth conditions as well as H<sup>+</sup>-inhibited growth rates, and that the carbon pool assimilates its carbon mainly from CO<sub>2</sub> (Hermoso, 2015). It is important to note, however, that the plateau between  $\Delta^{13}\text{C}_{\text{Coccolith}}$  values and  $\mu/\text{CO}_2$  (Fig. 6c) highlights either a notable contribution from HCO<sub>3</sub><sup>-</sup> uptake at lower [CO<sub>2</sub>], or a diffusive loss of isotopically light CO<sub>2</sub> from the intracellular pool. A similar change is also evident in  $\Delta^{13}\text{C}_{\text{CORG}}$  (Fig. S5), further suggesting a shared internal carbon pool.

Regarding  $\Delta^{18}\text{O}_{\text{Coccolith}}$  values, our observations align with the isotopic pattern of pH-corrected inorganic calcite, albeit influenced by a significant vital effect of  $\sim 2\text{‰}$  (Fig. 2b, 3b, 6d). This finding suggests that the calcite precipitation occurs in oxygen isotopic equilibrium with the DIC, and the intracellular carbon pool comprises CO<sub>2</sub> fully isotopically equilibrated with H<sub>2</sub>O. The observed isotopic offset towards depleted values is attributed to elevated intracellular pH during calcification across all treatments, a phenomenon comparable to observations in *C. leptoporus*. This highlights the physiological similarity between *C. carterae* and *C. leptoporus* where an offset towards depleted values in  $\Delta^{18}\text{O}_{\text{Coccolith}}$  values and a  $\mu_{\text{opt}}$  at relatively higher CO<sub>2</sub> concentrations could be caused by a higher intracellular pH and long residence times for carbon allowing sufficient time for isotopic equilibration.

*C. carterae* stands out from the other species in this study, with a distinctive cellular composition characterised by a low PIC content and a high POC content (Gafar et al., 2019; McClelland et al., 2017). In conjunction with the propensity of this species for rapid calcite production (yielding potentially more than 100 coccoliths per cell), and a large intracellular carbon pool that is likely due to a large cell size, the relatively modest extraction from this pool (due to the low PIC content) ensures ample time for intracellular carbon pool replenishment and equilibration with the DIC-H<sub>2</sub>O system. Moreover, a small SA:V ratio due to its large cell size reduces the area available for unequilibrated CO<sub>2</sub> diffusion/leakage to take place (Table S1). This can be observed in the unchanging  $\Delta^{18}\text{O}_{\text{Coccolith}}$  values suggesting ample equilibration time for the oxygen isotopes across the different carbon species of the intracellular carbon pool, which is generally the rate limiting equilibration within the calcification fluid-DIC-H<sub>2</sub>O system. Additionally, high carbonic anhydrase activity can cause rapid isotopic equilibration and therefore, alleviate kinetic isotope effects (Uchikawa and Zeebe, 2012; Thaler et al., 2017).

#### 4.3. Trends in carbon and oxygen isotopes as a measure of species-specific intracellular carbon residence times

Interrogation of the data indicated a relationship between the

species-specific gradient of the  $\Delta^{13}\text{C}_{\text{Coccolith}}$  vs.  $\Delta^{18}\text{O}_{\text{Coccolith}}$  relationship, and the gradient of the  $\Delta^{13}\text{C}_{\text{CORG}}$  vs.  $\Delta^{13}\text{C}_{\text{Coccolith}}$  relationship (Fig. 7a). The residence time of carbon in an internal carbon pool may be the unifying factor driving this correlation. Carbon residence time is controlled by either the size of the internal pool and/or the rate of supply/demand (Hermoso et al., 2016b). The steepness of the  $\Delta^{13}\text{C}_{\text{Coccolith}}$  vs.  $\Delta^{18}\text{O}_{\text{Coccolith}}$  gradient is likely driven in part by the time available for equilibration of oxygen isotopes amongst all the carbon ionic species and water, the longest equilibration time among the isotope systems (Zeebe and Wolf-Gladrow, 2001). Further, the degree to which carbon utilisation of an internal carbon pool drives Rayleigh fractionation within that internal carbon pool, and whether calcification and photosynthesis draw from an isotopically similar carbon pool also acts as measures of the residence time of carbon inside the cell (Bolton and Stoll, 2013; Hermoso, 2015; Hermoso et al., 2016b; Holtz et al., 2015; Rickaby et al., 2010; Sekino and Shiraiwa, 1996).

The  $\Delta^{13}\text{C}_{\text{Coccolith}}$  and  $\Delta^{18}\text{O}_{\text{Coccolith}}$  values of coccolith calcite can be compared against theoretical maximums of pH-related and CO<sub>2</sub>-diffusion-related change in  $\Delta^{13}\text{C}_{\text{Coccolith}}$  and  $\Delta^{18}\text{O}_{\text{Coccolith}}$  values (Fig. 7a; Chen et al., 2018). pH-related depletion in  $\delta^{18}\text{O}$  values is a primary process that influences stable isotopes in coccolith calcite and is given by a horizontal slope (slope = 0; Zeebe, 1999). However, it is important to note that pH does not influence the  $\delta^{13}\text{C}$  values of calcite, despite the distinct isotopic compositions of various DIC species because, within an isotopically closed system, any alterations in  $\delta^{13}\text{C}$  solely result from shifts in the  $\delta^{13}\text{C}$  of the overall DIC (e.g., by adding or removing carbon of a certain  $\delta^{13}\text{C}$  value; Zeebe and Wolf-Gladrow, 2001).

Another theoretical maximum can be given by diffusive CO<sub>2</sub> that influences stable isotopes in coccolith calcite (Chen et al., 2018). This process primarily results in a depletion of  $\delta^{13}\text{C}$  values, provided that equilibration is established between diffusive CO<sub>2</sub> and the DIC-H<sub>2</sub>O system (Fig. 7a-inset). This depletion occurs because the  $\delta^{13}\text{C}$  of CO<sub>2</sub> is  $\sim 9\text{‰}$  more depleted than HCO<sub>3</sub><sup>-</sup>. The introduction of CO<sub>2</sub> to an isotopically closed system (e.g., intracellular carbon pool) results in an overall depletion of the  $\delta^{13}\text{C}$  in the system in proportion to the amount of carbon therein. Furthermore, the equilibration of H<sub>2</sub>O and CO<sub>2</sub> causes isotopic equilibration in  $\delta^{18}\text{O}$  values, but with slow (pH-dependent) kinetics, thus yielding a vertical slope (slope = infinity, Fig. 7a-inset; Zeebe and Wolf-Gladrow, 2001). Under non-equilibrium conditions between diffusive CO<sub>2</sub> and H<sub>2</sub>O, the  $\delta^{18}\text{O}$  of CO<sub>2</sub> is heavier than that of CO<sub>3</sub><sup>2-</sup>, HCO<sub>3</sub><sup>-</sup> and H<sub>2</sub>O (Zeebe and Wolf-Gladrow, 2001).

The emergence of a linear trend with a finite, non-zero slope in this dataset is a result of kinetic isotope effects impacting both  $\delta^{18}\text{O}$  and  $\delta^{13}\text{C}$  (Adkins et al., 2003; Chen et al., 2018; McConnaughey, 1989b, 1989a). Two primary processes contributing to these kinetic isotope effects have

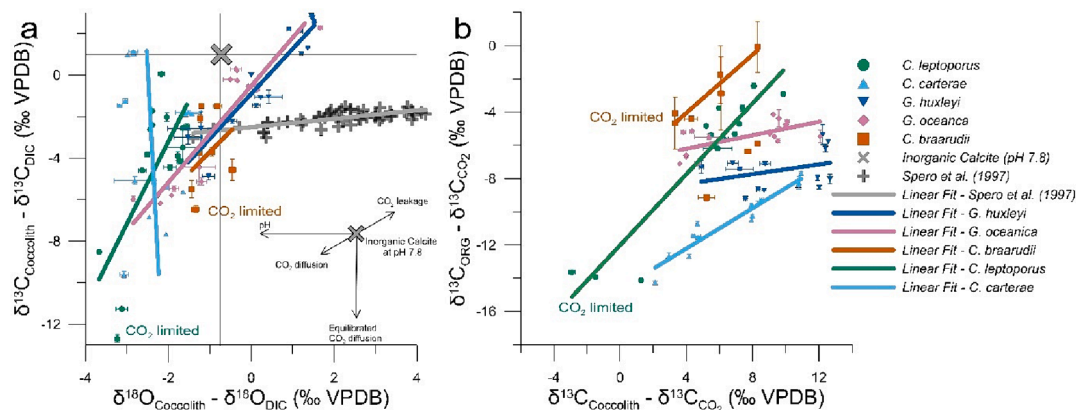


**Fig. 7.** (a)  $\Delta^{18}\text{O}_{\text{Coccolith}}$  vs.  $\Delta^{13}\text{C}_{\text{Coccolith}}$  for *C. braarudii* (■), *C. leptoporus* (●), *C. carterae* (▲), *G. huxleyi* (▼), and *G. oceanica* (◆). Data from Spero et al. (1997) (+) and inorganic calcite (×) has been included for comparison. The vector diagram (inset) shows the isotopic effects of unequilibrated CO<sub>2</sub> diffusion (diffusion of 9‰ depleted CO<sub>2</sub> and diffusion related CO<sub>2</sub> fractionation), CO<sub>2</sub> leakage and photosynthetic uptake, and pH. (b)  $\Delta^{13}\text{C}_{\text{Coccolith}}$  vs.  $\Delta^{13}\text{C}_{\text{CORG}}$ . Note that the  $\Delta^{13}\text{C}_{\text{CORG}}$  gradients for *C. braarudii* and *C. leptoporus* are calculated using  $\Delta^{13}\text{C}_{\text{CORG}}$  values at CO<sub>2</sub>-limiting and values at the lowest non-limiting CO<sub>2</sub> concentrations.

been identified in this study: (unequilibrated) CO<sub>2</sub> diffusion, and CO<sub>2</sub> leakage related fractionation (Fig. 7a-inset). The unequilibrated diffusion of CO<sub>2</sub> across the cell membrane is driven by concentration gradients, which lead to depletions in both δ<sup>18</sup>O and δ<sup>13</sup>C compared to the residual reservoir (i.e., ambient seawater). Furthermore, isotopic fractionations in the diffusing CO<sub>2</sub> are a consequence of the isotopic composition of CO<sub>2</sub> (depleted in δ<sup>13</sup>C, enriched in δ<sup>18</sup>O compared to DIC), which is coupled with the kinetic isotope effects of diffusion (depletion in both δ<sup>13</sup>C and δ<sup>18</sup>O; O'Leary, 1984; Thiagarajan et al., 2011; Zeebe and Wolf-Gladrow, 2001). Moreover, δ<sup>18</sup>O of the diffusing CO<sub>2</sub> can equilibrate with intracellular H<sub>2</sub>O. The combination of these processes leads to a more substantial depletion in δ<sup>13</sup>C than δ<sup>18</sup>O.

If complete equilibration of δ<sup>18</sup>O of CO<sub>2</sub> in the intracellular carbon pool with the ambient seawater results in a vertical slope, the gradients observed here can be attributed to the extent of equilibration between the intracellular carbon pools and the DIC-H<sub>2</sub>O system. This in turn, serves as an indicator of the residence time of the intracellular carbon pool (Fig. 7a). The gradient between Δ<sup>13</sup>C<sub>Coccolith</sub> and Δ<sup>18</sup>O<sub>Coccolith</sub> values can be calculated as follows (Table S3):

$$\text{Residence Time} \propto \frac{\Delta^{13}\text{C}_{\text{Coccolith}}}{\Delta^{18}\text{O}_{\text{Coccolith}}} = \frac{\text{Min}(\Delta^{13}\text{C}_{\text{Coccolith}}) - \text{Max}(\Delta^{13}\text{C}_{\text{Coccolith}})}{\text{Min}(\Delta^{18}\text{O}_{\text{Coccolith}}) - \text{Max}(\Delta^{18}\text{O}_{\text{Coccolith}})}$$

As previously discussed, the pronounced correlation between Δ<sup>13</sup>C<sub>Coccolith</sub> and Δ<sup>18</sup>O<sub>Coccolith</sub> values for *G. oceanica* and *G. huxleyi* arise due to kinetic isotope effects as a consequence of the short residence time for carbon within their intracellular carbon pool (Fig. 7a, 8; McConnaughey 1989a). Conversely, Δ<sup>13</sup>C<sub>Coccolith</sub> and Δ<sup>18</sup>O<sub>Coccolith</sub> values for *C. braarudii* are a consequence of long residence times for carbon, and intracellular pH buffered with the ambient pH. *C. leptoporus* exhibits long residence times for carbon in its relatively smaller internal carbon pool due to elevated intracellular pH compared to the ambient seawater. *C. braarudii* and *C. leptoporus* produce relatively steep

gradients in their Δ<sup>13</sup>C<sub>Coccolith</sub> and Δ<sup>18</sup>O<sub>Coccolith</sub> values due to isotopic depletion caused by CO<sub>2</sub> diffusion under CO<sub>2</sub>-limiting conditions (Fig. 7a, 8). Finally, *C. carterae* exhibits a large and well-equilibrated internal carbon pool with long residence times for carbon (Fig. 8). Similar to *C. leptoporus*, *C. carterae* shows elevated intracellular pH, as evidenced by its consistently depleted Δ<sup>18</sup>O<sub>Coccolith</sub> values (Fig. 7a). Notably, *C. carterae* exhibits a near-vertical slope, i.e., minimal change in δ<sup>18</sup>O with a trend closely resembling equilibrated diffusive CO<sub>2</sub>, characterised by δ<sup>13</sup>C depletion solely due to addition of (9‰ depleted) CO<sub>2</sub>.

Gradients between Δ<sup>13</sup>C<sub>ORG</sub> and Δ<sup>13</sup>C<sub>Coccolith</sub> values for each species can also offer insights into the internal dynamics of the intracellular carbon pool (Fig. 7b). A steep gradient (e.g., *C. carterae*) implies a shared carbon pool between calcification and organic matter fixation such that each process draws from the same carbon pool, while a shallow gradient (e.g., *G. huxleyi*) suggests a decoupling of these processes due to a short residence time of carbon within the intracellular carbon pool. Therefore, the gradient between Δ<sup>13</sup>C<sub>ORG</sub> and Δ<sup>13</sup>C<sub>Coccolith</sub> is directly proportional to the residence time of carbon within the intracellular carbon pool, and can be calculated as follows (Fig. 7b; Table S3):

$$\text{Residence Time} \propto \frac{\Delta^{13}\text{C}_{\text{ORG}}}{\Delta^{13}\text{C}_{\text{Coccolith}}} = \frac{\text{Min}(\Delta^{13}\text{C}_{\text{ORG}}) - \text{Max}(\Delta^{13}\text{C}_{\text{ORG}})}{\text{Min}(\Delta^{13}\text{C}_{\text{Coccolith}}) - \text{Max}(\Delta^{13}\text{C}_{\text{Coccolith}})}$$

<sup>a</sup>Note that the gradient is calculated using Δ<sup>13</sup>C<sub>ORG</sub> values at CO<sub>2</sub> concentrations of 2.83 μmol kg<sup>-1</sup> (CO<sub>2</sub>-limiting) and 11.13 μmol kg<sup>-1</sup> (lowest non-limiting CO<sub>2</sub> concentration) for *C. braarudii*. This choice is made because Δ<sup>13</sup>C<sub>ORG</sub> values again show depletion with increasing CO<sub>2</sub> (Fig. 2c, 7b).

The relationship between the gradients of Δ<sup>13</sup>C<sub>Coccolith</sub> vs. Δ<sup>18</sup>O<sub>Coccolith</sub> and Δ<sup>13</sup>C<sub>ORG</sub> vs. Δ<sup>13</sup>C<sub>Coccolith</sub> can therefore be used as two independent measurements for characterising species-specific residence time of carbon within the intracellular carbon pool (Fig. 9). The carbon

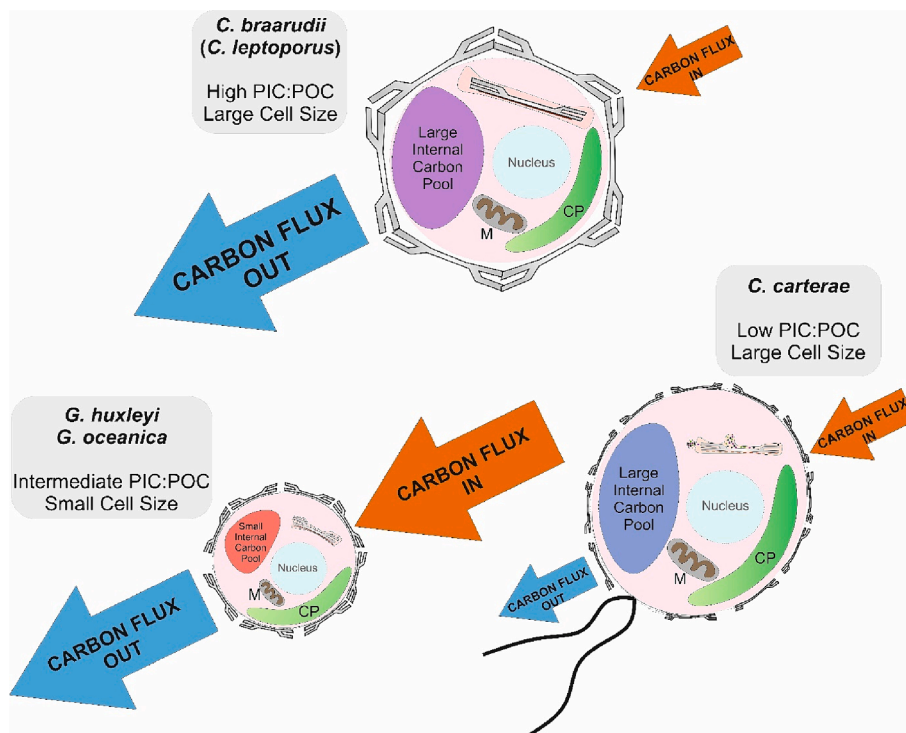


**Fig. 8.** A diagram elucidating the three primary carbon regulation categories identified in this study. The magnitude of the blue and orange arrows signifies the extent of carbon fluxes, with inflows and outflows regulated by the SA:V ratio and PIC:POC ratio, respectively. The size of the internal carbon pool corresponds to cell size, and the colour of the internal carbon pool signifies its ability to raise intracellular pH (blue – higher pH; purple – pH similar to ambient; red – pH lowered by CO<sub>2</sub> fluxes). Although *C. leptoporus* is categorised alongside *C. braarudii* because of its high PIC:POC ratios and similarity in isotopic trends, it serves as an intermediary between *C. braarudii* and *C. carterae*. This positioning is attributed to its capacity to elevate intracellular pH akin to *C. carterae*. M: mitochondrion, CP: Chloroplast.

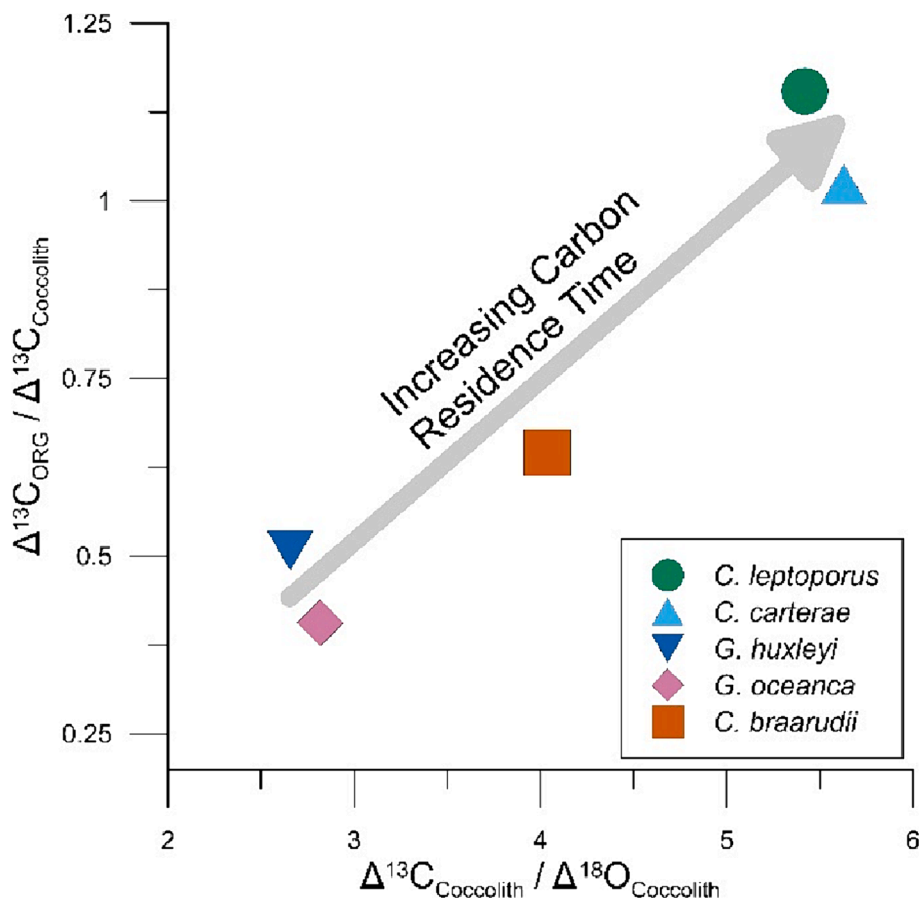


Fig. 9. A plot between  $\Delta^{13}\text{C}_{\text{Coccolith}}$  vs.  $\Delta^{18}\text{O}_{\text{Coccolith}}$  and  $\Delta^{13}\text{C}_{\text{ORG}}$  vs.  $\Delta^{13}\text{C}_{\text{Coccolith}}$  values as two independent measurements of species-specific residence time for carbon in the intracellular carbon pool. Note that the  $\Delta^{13}\text{C}_{\text{ORG}}$  gradients for *C. braarudii* and *C. leptoporus* are calculated using  $\Delta^{13}\text{C}_{\text{ORG}}$  values at  $\text{CO}_2$ -limiting and values at the lowest non-limiting  $\text{CO}_2$  concentrations.

residence times obtained from this method agree with studies that have previously quantified the size of the internal carbon pool using stable isotopes. For instance, in agreement with Hermoso et al. (2016), this study suggested that high  $\text{CO}_2$  diffusion into the cell leads to heavy  $\delta^{18}\text{O}_{\text{Coccolith}}$  values and small cell size (high SA:V ratio, Table S1) results in short residence times for carbon in the cell. Additionally, this study shows that the  $\text{CO}_2$  is the primary carbon substrate for the internal carbon pool; and that the degree of utilisation of the carbon pool (e.g., through PIC production) determines the extent of equilibration possible for its isotopes with the ambient DIC and  $\text{H}_2\text{O}$ , such that for species with large internal carbon pools, long carbon residence time allows re-equilibration of its isotopes, especially under non- $\text{CO}_2$  limiting conditions (Hermoso, 2015, 2014).

The differential isotopic responses across various coccolithophore species presented in this study can offer a valuable tool to understand the dynamics of carbon regulation in coccolithophores that reveal susceptibility to environmental change and can be used to trace changing physiology in response to past environmental change. With recent insights into the mechanism of coccolith calcification in *G. huxleyi*, the diffusion-limited rates of calcification provide further insights into the turnover times for carbon in a small coccolithophore cell (Avrahami et al., 2023). Furthermore, species-specific responses of coccolithophores to varying  $\text{CO}_2$  concentrations have implications for understanding how these organisms might fare in the face of ocean acidification. This study contributes to a more comprehensive view of the geochemical dynamics that lead to vital effects and highlights the use of stable isotopes as a tool to understand the mechanisms of carbon regulation within coccolithophores and broadly for phytoplankton. Organisms such as coccolithophores, with a calcification regime akin to a

“closed system” due to their intracellular calcification mechanism provide significant differences to “open system” calcifying organisms such as foraminifers and corals. By harnessing clumped isotopes, numerical modelling and isotopic analyses on a finer scale, the implications of this work can be expanded to unravel carbon regulation in more complex organisms, thereby providing insights into the marine carbon cycle.

## 5. Summary

This study provides insights into the isotopic responses of coccolithophores to changing environmental conditions. The findings gleaned from this research, which employs carbon and oxygen isotopic approaches, show that isotopic gradients between  $\Delta^{13}\text{C}_{\text{Coccolith}} - \Delta^{18}\text{O}_{\text{Coccolith}}$  values and  $\Delta^{13}\text{C}_{\text{Coccolith}} - \Delta^{13}\text{C}_{\text{ORG}}$  values offer a quantitative indicator of the residence time of carbon within the intracellular carbon pool. This residence time plays a critical role in the physiological dynamics of coccolithophores, and the size of this internal carbon pool is proportional to the size of the coccolithophore cell. Moreover, certain species, such as *C. carterae* and *C. leptoporus* can elevate their intracellular pH to minimise  $\text{CO}_2$  leakage. An exception to the cell size – internal carbon pool size relationship is *G. huxleyi*, which likely has a carbon pool larger than that of *G. oceanica* despite having a smaller cell size. This is evidenced by the isotopic offsets in the calcite and organic matter, which are heavier in the coccolith calcite for *G. huxleyi* compared to *G. oceanica*. Such an offset can be brought forward if *G. huxleyi* has a larger internal carbon pool, perhaps due to better  $\text{HCO}_3^-$  transport that allows better equilibration at high  $\text{CO}_2$ , but the larger carbon pool causes more  $\text{CO}_2$  loss under low  $\text{CO}_2$  conditions due to its higher SA:V ratio (due to the small cell size) compared to *G. oceanica*.

The decoupling of carbon isotopes in calcite and organic matter for *G. huxleyi* and *G. oceanica* suggest a short residence time for carbon and a small size of the internal carbon pool. On the other extreme lies *C. carterae*, which exhibits extended residence times for carbon and the capacity for full equilibration. Such observations underscore species-specific nature of carbon residence times, reflecting a spectrum of physiologies in coccolithophores and possibly broadly in phytoplankton communities.

### CRedit authorship contribution statement

**Nishant Chauhan:** Writing – review & editing, Writing – original draft, Data curation, Conceptualization. **Rosalind E.M. Rickaby:** Supervision, Funding acquisition, Formal analysis, Conceptualization.

### Data availability

Data are available through Zenodo at <https://zenodo.org/doi/10.5281/zenodo.8265649>.

### Declaration of competing interest

The authors declare that they have no known competing financial interests or personal relationships that could have appeared to influence the work reported in this paper.

### Acknowledgements

The project was supported by funding from the European Research Council (ERC) under the European Union's Horizon 2020 research and innovation program (SCOOBI project, grant agreement no. 101019146; RER) and from the Natural Environment Research Council (NERC; PUGCA project, award NE/V011049/1; RER). NC was supported by the Clarendon fund and St. John's College, University of Oxford. This study has used research infrastructure facilities provided by University of Oxford and University of Southampton and we are grateful to Christopher Day and Bastian Hambach for their expertise with the stable isotope analyses. No conflicts of interest are declared.

### Appendix A. Supplementary material

The supplementary material contains a detailed description of specific methodologies used in this study. We have also discussed our results with previous studies in the Results section (with corresponding plots). Additionally, plots (e.g., growth rates,  $\Delta^{13}\text{C}_{\text{Coccolith}}$  and  $\Delta^{18}\text{O}_{\text{Coccolith}}$ , and  $\Delta^{13}\text{C}_{\text{ORG}}$ ) from the main document have been replotted to show every biological replicate, instead of their averages. The tables contain calculated stable isotope values of inorganic calcite based on Zeebe (1999), Kim & O'Neil (1997) and Watkins et al. (2013), and auxiliary data (e.g., cell dimensions, PIC:POC) for the coccolithophore species used in this study. Supplementary material to this article can be found online at <https://doi.org/10.1016/j.gca.2024.03.033>.

### References

Adkins, J.F., Boyle, E.A., Curry, W.B., Lutringer, A., 2003. Stable isotopes in deep-sea corals and a new mechanism for "vital effects". *Geochim. Cosmochim. Acta* 67, 1129–1143.

Agnini, C., Fornaciari, E., Rio, D., Raffi, I., Catanzariti, R., Pälke, H., Backman, J., 2014. A new low-to middle-latitude biozonation and revised biochronology of palaeogene calcareous nannofossils biozonation and biochronology of paleogene calcareous nannofossils from low and middle latitudes. *Newsl. Stratigr.* 47, 131–181.

Andersen, R., 2005. *Algal culturing techniques*. Elsevier.

Anning, T., Nimer, N., Merrett, M.J., Brownlee, C., 1996. Costs and benefits of calcification in coccolithophorids. *J. Mar. Syst.* 9, 45–56.

Avrahami, E.M., Eyal, Z., Varsano, N., Zagoriy, I., Mahamid, J., Gal, A., 2023. Transport-Limited Growth of Coccolith Crystals. *Advanced Materials* 2309547.

Bach, L.T., Riebesell, U., Schulz, K.G., 2011. Distinguishing between the effects of ocean acidification and ocean carbonation in the coccolithophore *Emiliania huxleyi*. *Limnol. Oceanogr.* 56, 2040–2050.

Bach, L.T., MacKinder, L.C.M., Schulz, K.G., Wheeler, G., Schroeder, D.C., Brownlee, C., Riebesell, U., 2013. Dissecting the impact of CO<sub>2</sub> and pH on the mechanisms of photosynthesis and calcification in the coccolithophore *Emiliania huxleyi*. *New Phytol.* 199, 121–134.

Bach, L., Riebesell, U., Gutowska, M.A., Federwisch, L., Schulz, K.G., 2015. A unifying concept of coccolithophore sensitivity to changing carbonate chemistry embedded in an ecological framework. *Prog. Oceanogr.* 135, 125–138.

Backman, J., 1980. Miocene-Pliocene nannofossils and sedimentation rates in the Hatton-Rockall Basin. *NE Atlantic Ocean*.

Balch, W.M., Kilpatrick, K., Holligan, P.M., Cucci, T., 1993. Coccolith Production and Detachment By *Emiliania huxleyi* (prymnesiophyceae)1. *J. Phycol.* 29, 566–575.

Bendif, E.M., Nevado, B., Wong, E.L.Y., Hagino, K., Probert, I., Young, J.R., Rickaby, R.E.M., Filatov, D.A., 2019. Repeated species radiations in the recent evolution of the key marine phytoplankton lineage *Gephyrocapsa*. *Nature Communications* 2019 10: 1 10, 1–9.

Boller, A.J., Thomas, P.J., Cavanaugh, C.M., Scott, K.M., 2011. Low stable carbon isotope fractionation by coccolithophore *RubisCO*. *Geochim. Cosmochim. Acta* 75, 7200–7207.

Bolton, C.T., Stoll, H.M., 2013. Late Miocene threshold response of marine algae to carbon dioxide limitation. *Nature* 2013 500:7464 500, 558–562.

Bolton, C.T., Hernández-Sánchez, M.T., Fuertes, M.A., González-Lemos, S., Abrevaya, L., Mendez-Vicente, A., Flores, J.A., Probert, I., Giosan, L., Johnson, J., Stoll, H.M., 2016. Decrease in coccolithophore calcification and CO<sub>2</sub> since the middle Miocene. *Nature Communications* 2016 7:1 7, 1–13.

Bown, P.R., Lees, J.A., Young, J.R., 2004. Calcareous nannoplankton evolution and diversity through time. *Coccolithophores* 481–508.

Burkhardt, S., Riebesell, U., Zondervan, I., 1999a. Effects of growth rate, CO<sub>2</sub> concentration, and cell size on the stable carbon isotope fractionation in marine phytoplankton. *Geochim. Cosmochim. Acta* 63, 3729–3741.

Burkhardt, S., Riebesell, U., Zondervan, I., 1999b. Stable carbon isotope fractionation by marine phytoplankton in response to daylength, growth rate, and CO<sub>2</sub> availability. *Mar. Ecol. Prog. Ser.* 184, 31–41.

Chen, S., Gagnon, A.C., Adkins, J.F., 2018. Carbonic anhydrase, coral calcification and a new model of stable isotope vital effects. *Geochim. Cosmochim. Acta* 236, 179–197.

Claxton, L.M., McClelland, H.L.O., Hermoso, M., Rickaby, R.E.M., 2022. Eocene emergence of highly calcifying coccolithophores despite declining atmospheric CO<sub>2</sub>. *Nature Geoscience* 2022 15:10 15, 826–831.

Daniels, C.J., Sheward, R.M., Poulton, A.J., 2014. Biogeochemical implications of comparative growth rates of *Emiliania huxleyi* and *Coccolithus* species. *Biogeosciences* 11, 6915–6925.

Dickson, A.G., Millero, F.J., 1987. A comparison of the equilibrium constants for the dissociation of carbonic acid in seawater media. *Deep Sea Res. Part A Oceanographic Res. Pap.* 34, 1733–1743.

Dudley, W.C., Blackwelder, P., Brand, L., Duplessy, J.C., 1986. Stable isotopic composition of coccoliths. *Mar. Micropaleontol.* 10, 1–8.

Eiler, J.M., 2007. "Clumped-isotope" geochemistry—The study of naturally-occurring, multiply-substituted isotopologues. *Earth Planet. Sci. Lett.* 262, 309–327.

Feng, Y., Roleda, M.Y., Armstrong, E., Boyd, P.W., Hurd, C.L., 2017. Environmental controls on the growth, photosynthetic and calcification rates of a Southern Hemisphere strain of the coccolithophore *Emiliania huxleyi*. *Limnol. Oceanogr.* 62, 519–540.

Fiorini, S., Middelburg, J., J.G.-J. 2011. Testing the effects of elevated pCO<sub>2</sub> on coccolithophores (Prymnesiophyceae): Comparison between haploid and diploid life stages 1. *Wiley Online Library* 47, 1281–1291.

Gafar, Natasha A., Eyre, B.D., Schulz, K.G., 2019. A comparison of species specific sensitivities to changing light and carbonate chemistry in calcifying marine phytoplankton. *Scientific Reports* 2019 9:1 9, 1–12.

Gafar, N.A., Eyre, B.D., Schulz, K.G., 2019a. Particulate inorganic to organic carbon production as a predictor for coccolithophorid sensitivity to ongoing ocean acidification. *Limnol. Oceanogr. Lett.* 4, 62–70.

González-Lanchas, A., Hernández-Almeida, I., Flores, J.A., Sierro, F.J., Guitian, J., Stoll, H.M., 2021. Carbon isotopic fractionation of alkenones and *gephyrocapsa* coccoliths over the late quaternary (Marine Isotope Stages 12–9) glacial-interglacial cycles at the Western Tropical Atlantic. *Paleoceanogr. Paleoclimatol.* 36.

Guillard, R.R., Ryther, J.H., 1962. Studies of marine planktonic diatoms: I. *Cyclotella nana* Husted, and *Detonula confervacea* (Cleve) Gran. *Can. J. Microbiol.* 8, 229–239.

Guy, R.D., Fogel, M.L., Berry, J.A., 1993. Photosynthetic fractionation of the stable isotopes of oxygen and carbon. *Plant Physiol.* 101, 37–47.

Halloran, P.R., Hall, I.R., Colmenero-Hidalgo, E., M. Rickaby, R.E., 2008. Evidence for a multi-species coccolith volume change over the past two centuries: Understanding a potential ocean acidification response. *Biogeosciences* 5, 1651–1655.

Henderiks, J., Pagani, M., 2008. Coccolithophore cell size and the Paleogene decline in atmospheric CO<sub>2</sub>. *Earth Planet. Sci. Lett.* 269, 576–584.

Hermoso, M., 2014. Coccolith-derived isotopic proxies in palaeoceanography: where geologists need biologists. *Cryptogam. Algal.* 35, 323–351.

Hermoso, M., 2015. Control of ambient pH on growth and stable isotopes in phytoplanktonic calcifying algae. *Paleoceanography* 30, 1100–1112.

Hermoso, M., Chan, I.Z.X., McClelland, H.L.O., Heurreux, A.M.C., Rickaby, R.E.M., 2016a. Vanishing coccolith vital effects with alleviated carbon limitation. *Biogeosciences* 13, 301–312.

Hermoso, M., Minoletti, F., Aloisi, G., Bonifacie, M., McClelland, H.L.O., Labourdette, N., Renforth, P., Chaduteau, C., Rickaby, R.E.M., 2016b. An explanation for the 18 O

- excess in Noelaerhabdaceae coccolith calcite. *Geochim. Cosmochim. Acta* 189, 132–142.
- Hermoso, M., McClelland, H.L.O., Hirst, J.S., Minoletti, F., Bonifacie, M., Rickaby, R.E. M., 2020. Towards the use of the coccolith vital effects in palaeoceanography: A field investigation during the middle Miocene in the SW Pacific Ocean. *Deep Sea Res. Part I* 160, 103262.
- Heureux, A., 2016. Carbon fixation in eukaryotic marine algae: Evolution of photosynthetic machinery and isotopic footprints. University of Oxford [PhD Thesis].
- Holtz, L.M., Wolf-Gladrow, D., Thoms, S., 2015. Numerical cell model investigating cellular carbon fluxes in *Emiliana huxleyi*. *J. Theor. Biol.* 364, 305–315.
- Holtz, L.M., Wolf-Gladrow, D., Thoms, S., 2017. Stable carbon isotope signals in particulate organic and inorganic carbon of coccolithophores – A numerical model study for *Emiliana huxleyi*. *J. Theor. Biol.* 420, 117–127.
- Hoppe, C.J.M., Langer, G., Rost, B., 2011. *Emiliana huxleyi* shows identical responses to elevated pCO<sub>2</sub> in TA and DIC manipulations. *J. Exp. Mar. Biol. Ecol.* 406, 54–62.
- Houdan, A., Bonnard, A., Fresnel, J., Fouchard, S., Billard, C., Probert, I., 2004. Toxicity of coastal coccolithophores (Prymnesiophyceae, Haptophyta). *J. Plankton Res.* 26, 875–883.
- Iglesias-Rodriguez, M.D., Halloran, P.R., Rickaby, R.E.M., Hall, I.R., Colmenero-Hidalgo, E., Gittins, J.R., Green, D.R.H., Tyrrell, T., Gibbs, S.J., Von Dassow, P., Rehm, E., Armbrust, E.V., Boessenkool, K.P., 2008. Phytoplankton calcification in a high-CO<sub>2</sub> world. *Science* 320, 336–340.
- Jähne, B., Heinz, G., Dietrich, W., 1987. Measurement of the diffusion coefficients of sparingly soluble gases in water. *J. Geophys. Res. Oceans* 92, 10767–10776.
- Kaplan, A., Reinhold, L., 2003. CO<sub>2</sub> Concentrating Mechanisms in photosynthetic microorganisms. *Annu. Rev. Plant. Physiol. Plant. Mol. Biol.* 50, 539–570.
- Keller, M.D., Guillard, R.R.L., 1985. Factors significant to marine dinoflagellate culture. Elsevier, New York.
- Keller, K., Morel, F.M.M., 1999. A model of carbon isotopic fractionation and active carbon uptake in phytoplankton. *Mar. Ecol. Prog. Ser.* 182, 295–298.
- Keller, M.D., Selvin, R.C., Claus, W., Guillard, R.R., 1987. Media for the culture of oceanic ultraphytoplankton. *J. Phycol.* 23, 633–638.
- Kim, S.T., O'Neil, J.R., 1997. Equilibrium and nonequilibrium oxygen isotope effects in synthetic carbonates. *Geochim. Cosmochim. Acta* 61, 3461–3475.
- Kottmeier, D.M., Chrachri, A., Langer, G., Helliwell, K.E., Wheeler, G.L., Brownlee, C., 2022. Reduced H<sup>+</sup> channel activity disrupts pH homeostasis and calcification in coccolithophores at low ocean pH. *PNAS* 119.
- Kottmeier, D., Rokitta, S.D., Tortell, P.D., Rost, B., 2014. Strong shift from HCO<sub>3</sub><sup>-</sup> to CO<sub>2</sub> uptake in *Emiliana huxleyi* with acidification: New approach unravels acclimation versus short-term pH effects. *Photosynth. Res.* 121, 265–275.
- Kottmeier, D.M., Rokitta, S.D., Rost, B., 2016a. H<sup>+</sup>-driven increase in CO<sub>2</sub> uptake and decrease in HCO<sub>3</sub><sup>-</sup> uptake explain coccolithophores' acclimation responses to ocean acidification. *Limnol. Oceanogr.* 61, 2045–2057.
- Kottmeier, D.M., Rokitta, S.D., Rost, B., 2016b. Acidification, not carbonation, is the major regulator of carbon fluxes in the coccolithophore *Emiliana huxleyi*. *New Phytol.* 211, 126–137.
- Krug, S., Schulz, K., Riebesell, U., 2011. Effects of changes in carbonate chemistry speciation on *Coccolithus braurudii*: a discussion of coccolithophorid sensitivities. [bg.copernicus.org](http://bg.copernicus.org) 8, 771–777.
- Langer, G., Bode, M., 2011. CO<sub>2</sub> mediation of adverse effects of seawater acidification in *Calcidiscus leptoporus*. *Geochem. Geophys. Geosyst.* 12 n/a-n/a.
- Langer, G., Geisen, M., Baumann, K.H., Kläs, J., Riebesell, U., Thoms, S., Young, J.R., 2006. Species-specific responses of calcifying algae to changing seawater carbonate chemistry. *Geochemistry, Geophysics, Geosystems* 7.
- Langer, G., Nehrke, G., Probert, I., Ly, J., Ziveri, P., 2009. Strain-specific responses of *Emiliana huxleyi* to changing seawater carbonate chemistry. *Biogeosciences* 6, 2637–2646.
- LaRoche, J., Rost, B., Engel, A., 2010. Bioassays, batch culture and chemostat experimentation. In *Approaches and tools to manipulate the carbonate chemistry., Guide for Best Practices in Ocean Acidification Research and Data Reporting.* 81–94.
- Laws, E.A., Popp, B.N., Bidigare, R.R., Kennicutt, M.C., Macko, S.A., 1995. Dependence of phytoplankton carbon isotopic composition on growth rate and [CO<sub>2</sub>]<sub>aq</sub>: Theoretical considerations and experimental results. *Geochim. Cosmochim. Acta* 59, 1131–1138.
- Laws, E.A., Thompson, P.A., Popp, B.N., Bidigare, R.R., 1998. Sources of inorganic carbon for marine microalgal photosynthesis: A reassessment of δ<sup>13</sup>C data from batch culture studies of *Thalassiosira pseudonana* and *Emiliana huxleyi*. *Limnol. Oceanogr.* 43, 136–142.
- Laws, E.A., Popp, B.N., Cassar, N., Tanimoto, J., 2002. 13C discrimination patterns in oceanic phytoplankton: likely influence of CO<sub>2</sub> concentrating mechanisms, and implications for palaeoreconstructions. *Funct. Plant Biol.* 29, 323–333.
- Lee, R.B.Y., Mavridou, D.A.I., Papadakis, G., McClelland, H.L.O., Rickaby, R.E.M., 2016. The uronic acid content of coccolith-associated polysaccharides provides insight into coccolithogenesis and past climate. *Nat. Commun.* 7.
- Liu, Y.W., Eagle, R.A., Aciego, S.M., Gilmore, R.E., Ries, J.B., 2018. A coastal coccolithophore maintains pH homeostasis and switches carbon sources in response to ocean acidification. *Nat. Commun.* 9.
- Liu, Y.W., Rokitta, S.D., Rost, B., Eagle, R.A., 2021. Constraints on coccolithophores under ocean acidification obtained from boron and carbon geochemical approaches. *Geochim. Cosmochim. Acta* 315, 317–332.
- Mackinder, L., Wheeler, G., Schroeder, D., Riebesell, U., Brownlee, C., 2010. Molecular mechanisms underlying calcification in coccolithophores. *Geomicrobiol. J.* 27, 585–595.
- McClelland, H.L.O., Bruggeman, J., Hermoso, M., Rickaby, R.E.M., 2017. The origin of carbon isotope vital effects in coccolith calcite. *Nature Communications* 2017 8:1 8, 1–16.
- McConnaughey, T., 1989a. 13C and 18O isotopic disequilibrium in biological carbonates: I. Patterns. *Geochim. Cosmochim. Acta* 53, 151–162.
- McConnaughey, T., 1989b. 13C and 18O isotopic disequilibrium in biological carbonates: II. In vitro simulation of kinetic isotope effects. *Geochim. Cosmochim. Acta* 53, 163–171.
- McConnaughey, T.A., 2003. Sub-equilibrium oxygen-18 and carbon-13 levels in biological carbonates: Carbonate and kinetic models. *Coral Reefs* 22, 316–327.
- McCrea, J.M., 1950. On the isotopic chemistry of carbonates and a paleotemperature scale. *J. Chem. Phys.* 18, 849–857.
- Mehrbach, C., Culbertson, C., et al., 1973. Measurement of the apparent dissociation constants of carbonic acid in seawater at atmospheric pressure 1. *Wiley Online Library* 18, 897–907.
- Mook, W.G., Bommerson, J.C., Staverman, W.H., 1974. Carbon isotope fractionation between dissolved bicarbonate and gaseous carbon dioxide. *Earth Planet. Sci. Lett.* 22, 169–176.
- Morel, F., Rueter, J., et al., 1979. AQUIL: A chemically defined phytoplankton culture medium for trace metal studies. *Wiley Online Library* 15, 135–141.
- O'Leary, M.H., 1984. Measurement of the isotope fractionation associated with diffusion of carbon dioxide in aqueous solution. *J. Phys. Chem.* 88, 823–825.
- O'Leary, M.H., Madhavan, S., Paneth, P., 1992. Physical and chemical basis of carbon isotope fractionation in plants. *Plant Cell Environ.* 15, 1099–1104.
- Paasche, E., 1964. A tracer study of the inorganic carbon uptake during coccolith formation and photosynthesis in the coccolithophorid *Coccolithus huxleyi*. *Physiol. Plant Suppl.* 5–82.
- Paasche, E., 2001. A review of the coccolithophorid *Emiliana huxleyi* (Prymnesiophyceae), with particular reference to growth, coccolith formation, and calcification-photosynthesis interactions. *Phycologia* 40, 503–529.
- Pagani, M., 2002. The alkenone-CO<sub>2</sub> proxy and ancient atmospheric carbon dioxide. *Philos. Trans. Roy. Soc. Lond. Series A: Math., Phys. Eng. Sci.* 360, 609–632.
- Pierrot, D., Lewis, E., Wallace, D.W.R., 2006. MS Excel program developed for CO<sub>2</sub> system calculations. ORNL/CDIAC-105a.
- Price, N.M., Harrison, G.I., Hering, J.G., Hudson, R.J., Nirel, P.M.V., Palenik, B., Morel, F.M.M., 1989. Preparation and Chemistry of the artificial algal culture medium aquil. *Biol. Oceanogr.* 6, 443–461.
- Rau, G.H., Riebesell, U., Wolf-Gladrow, D., 1996. A model of photosynthetic <sup>13</sup>C fractionation by marine phytoplankton based on diffusive molecular CO<sub>2</sub> uptake. *Mar. Ecol. Prog. Ser.* 133, 275–285.
- Reinfelder, J.R., 2010. Carbon Concentrating Mechanisms in Eukaryotic Marine Phytoplankton. *Ann. Rev. Mar. Sci.* 3, 291–315.
- Rickaby, R., Henderiks, J., Young, J., 2010. Perturbing phytoplankton: response and isotopic fractionation with changing carbonate chemistry in two coccolithophore species. *Clim. Past* 6, 771–785.
- Ridgwell, A., 2005. A Mid Mesozoic Revolution in the regulation of ocean chemistry. *Mar. Geol.* 217, 339–357.
- Rokitta, S.D., Rost, B., 2012. Effects of CO<sub>2</sub> and their modulation by light in the life-cycle stages of the coccolithophore *Emiliana huxleyi*. *Limnol. Oceanogr.* 57, 607–618.
- Romanek, C.S., Grossman, E.L., Morse, J.W., 1992. Carbon isotopic fractionation in synthetic aragonite and calcite: Effects of temperature and precipitation rate. *Geochim. Cosmochim. Acta* 56, 419–430.
- Rost, B., Riebesell, U., Burkhardt, S., Sültemeyer, D., 2003. Carbon acquisition of bloom-forming marine phytoplankton. *Limnol. Oceanogr.* 48, 55–67.
- Rost, B., Riebesell, U., Sültemeyer, D., 2006. Carbon acquisition of marine phytoplankton: Effect of photoperiod length. *Limnol. Oceanogr.* 51, 12–20.
- Schauble, E.A., 2004. Applying Stable Isotope Fractionation Theory to New Systems. *Rev. Mineral. Geochem.* 55, 65–111.
- Sekino, K., Shiraiwa, Y., 1996. Evidence for the Involvement of Mitochondrial Respiration in Calcification in a Marine Coccolithophorid, *Emiliana huxleyi*. *Plant Cell Physiol.* 37, 1030–1033.
- Sett, S., Bach, L.T., Schulz, K.G., Koch-Klavsén, S., Lebrato, M., Riebesell, U., 2014. Temperature modulates coccolithophorid sensitivity of growth, photosynthesis and calcification to increasing seawater pCO<sub>2</sub>. *PLoS One* 9.
- Sikes, C.S., Roer, R.D., Wilbur, K.M., 1980. Photosynthesis and coccolith formation: Inorganic carbon sources and net inorganic reaction of deposition. *Limnol. Oceanogr.* 25, 248–261.
- Spero, H.J., Bijma, J., Lea, D.W., Bernis, B.E., 1997. Effect of seawater carbonate concentration on foraminiferal carbon and oxygen isotopes. *Nature* 1997 390:6659 390, 497–500.
- Stojkovic, S., Beardall, J., Matear, R., 2013. CO<sub>2</sub>-concentrating mechanisms in three southern hemisphere strains of *Emiliana huxleyi*. *J. Phycol.* 49, 670–679.
- Stoll, H.M., Guittán, J., Hernandez-Almeida, I., Mejía, L.M., Phelps, S., Polissar, P., Rosenthal, Y., Zhang, H., Ziveri, P., 2019. Upregulation of phytoplankton carbon concentrating mechanisms during low CO<sub>2</sub> glacial periods and implications for the phytoplankton pCO<sub>2</sub> proxy. *Quat. Sci. Rev.* 208, 1–20.
- Suffrian, K., Schulz, K.G., Gutowska, M.A., Riebesell, U., Bleich, M., 2011. Cellular pH measurements in *Emiliana huxleyi* reveal pronounced membrane proton permeability. *New Phytol.* 190, 595–608.
- Taylor, A.R., Chrachri, A., Wheeler, G., Goddard, H., Brownlee, C., 2011. A voltage-gated H<sup>+</sup> channel underlying pH homeostasis in calcifying Coccolithophores. *PLoS Biol.* 9.
- Tcherkez, G.G.B., Farquhar, G.D., Andrews, T.J., 2006. Despite slow catalysis and confused substrate specificity, all ribulose biphosphate carboxylases may be nearly perfectly optimized. *PNAS* 103, 7246–7251.

- Tchernov, D., Helman, Y., Keren, N., Luz, B., Ohad, I., Reinhold, L., Ogawa, T., Kaplan, A., 2001. Passive Entry of CO<sub>2</sub> and Its Energy-dependent Intracellular Conversion to HCO<sub>3</sub><sup>-</sup> in Cyanobacteria Are Driven by a Photosystem I-generated ΔμH<sup>+</sup>. *J. Biol. Chem.* 276, 23450–23455.
- Tchernov, D., Gruber, D.F., Irwin, A., 2014. Isotopic fractionation of carbon in the coccolithophorid *Emiliana huxleyi*. *Mar. Ecol. Prog. Ser.* 508, 53–66.
- Thaler, C., Millo, C., Ader, M., Chaduteau, C., Guyot, F., Ménez, B., 2017. Disequilibrium δ<sup>18</sup>O values in microbial carbonates as a tracer of metabolic production of dissolved inorganic carbon. *Geochim. Cosmochim. Acta* 199, 112–129.
- Thiagarajan, N., Adkins, J., Eiler, J., 2011. Carbonate clumped isotope thermometry of deep-sea corals and implications for vital effects. *Geochim. Cosmochim. Acta* 75, 4416–4425.
- Trimborn, S., Langer, G., Rost, B., 2007. Effect of varying calcium concentrations and light intensities on calcification and photosynthesis in *Emiliana huxleyi*. *Limnol. Oceanogr.* 52, 2285–2293.
- Uchikawa, J., Zeebe, R.E., 2012. The effect of carbonic anhydrase on the kinetics and equilibrium of the oxygen isotope exchange in the CO<sub>2</sub>–H<sub>2</sub>O system: Implications for δ<sup>18</sup>O vital effects in biogenic carbonates. *Geochim. Cosmochim. Acta* 95, 15–34.
- Urey, H., 1947. The thermodynamic properties of isotopic substances. *J. Chem. Soc.* 562–581.
- Venn, A., Tambutté, E., Holcomb, M., Allemand, D., Tambutté, S., 2011. Live tissue imaging shows reef corals elevate pH under their calcifying tissue relative to seawater. *PLoS One* 6, e20013.
- Walker, C.E., Taylor, A.R., Langer, G., Durak, G.M., Heath, S., Probert, I., Tyrrell, T., Brownlee, C., Wheeler, G.L., 2018. The requirement for calcification differs between ecologically important coccolithophore species. *New Phytol.* 220, 147–162.
- Wanner, P., Hunkeler, D., 2019. Isotope fractionation due to aqueous phase diffusion – What do diffusion models and experiments tell? – A review. *Chemosphere* 219, 1032–1043.
- Watkins, J.M., Nielsen, L.C., Ryerson, F.J., DePaolo, D.J., 2013. The influence of kinetics on the oxygen isotope composition of calcium carbonate. *Earth Planet. Sci. Lett.* 375, 349–360.
- Wheeler, G.L., Sturm, D., Langer, G., 2023. *Gephyrocapsa huxleyi* (*Emiliana huxleyi*) as a model system for coccolithophore biology. *J. Phycol.* 59, 1123–1129.
- Wilkes, E.B., Lee, R.B.Y., McClelland, H.L.O., Rickaby, R.E.M., Pearson, A., 2018. Carbon isotope ratios of coccolith-associated polysaccharides of *Emiliana huxleyi* as a function of growth rate and CO<sub>2</sub> concentration. *Org. Geochem.* 119, 1–10.
- Young, J.R., 1998. Neogene. In: Bown, P.R. (Ed.), *Calcareous Nannofossil Biostratigraphy*. British Micropalaeontological Society Publication Series, pp. 225–265.
- Zeebe, R.E., 1999. An explanation of the effect of seawater carbonate concentration on foraminiferal oxygen isotopes. *Geochim. Cosmochim. Acta* 63, 2001–2007.
- Zeebe, R.E., Wolf-Gladrow, D.A., 2001. CO<sub>2</sub> in seawater: equilibrium, kinetics, isotopes, *Book Series. Oceanography*, Elsevier.
- Zhang, H., Blanco-Ameijeiras, S., Hopkinson, B.M., Bernasconi, S.M., Mejia, L.M., Liu, C., Stoll, H., 2021. An isotope label method for empirical detection of carbonic anhydrase in the calcification pathway of the coccolithophore *Emiliana huxleyi*. *Geochim. Cosmochim. Acta* 292, 78–93.
- Zhang, Y., Gao, K., 2021. Photosynthesis and calcification of the coccolithophore *Emiliana huxleyi* are more sensitive to changed levels of light and CO<sub>2</sub> under nutrient limitation. *J. Photochem. Photobiol. B* 217.
- Ziveri, P., Thoms, S., Probert, I., Geisen, M., Langer, G., 2012. A universal carbonate ion effect on stable oxygen isotope ratios in unicellular planktonic calcifying organisms. *Biogeosciences* 9, 1025–1032.
- Zondervan, I., Rost, B., Riebesell, U., 2002. Effect of CO<sub>2</sub> concentration on the PIC/POC ratio in the coccolithophore *Emiliana huxleyi* grown under light-limiting conditions and different daylengths. *J. Exp. Mar. Biol. Ecol.* 272, 55–70.